Wenyu Zhou

Master's thesis

2021

Master's thesis

NTNU
Norwegian University of
Science and Technology
Faculty of Engineering
Department of Geoscience and Petroleum

NTNU
Norwegian University of
Science and Technology

Wenyu Zhou

Experimental Investigation of Osmosis and Spontaneous Emulsification During Low Salinity Flooding

August 2021

NTNU
Norwegian University of
Science and Technology

NTNU
Norwegian University of
Science and Technology

Experimental Investigation of Osmosis and Spontaneous Emulsification During Low Salinity Flooding

Wenyu Zhou

Petroleum engineering
Submission date: August 2021
Supervisor: Carl Fredrik Berg
Co-supervisor: Lifei Yan (Utrecht Univerisity)
Mohammad Hossein Golestan (NTNU)

Norwegian University of Science and Technology
Department of Geoscience and Petroleum

Abstract

This experimental study investigates the osmosis and the spontaneous emulsification as oil mobilization mechanisms during the low salinity water flooding by measuring the connate water expansion area in an oil-wet microfluidic system. Two types of synthetical oil, heptane and dodecane and different salinity brines are chosen to use in the experiments. Meanwhile, surfactants are added into the oil phase to calculate the water transportation rate due to the spontaneous emulsification, comparing with the water transportation rate due to the osmosis. Dynamic light scattering and pendant drop experiments were conducted with the same fluids to study the spontaneous emulsification process.

The HSW expansion due to the osmosis was observed at the microfluidic experiments with both heptane and dodecane under a salinity gradient. The water transportation rate for the osmosis is as high as the rate for the spontaneous emulsification with the enough amounts of surfactants added into the heptane. Insufficient surfactants added may inhibits the water transportation in the synthetic oil. The dodecane shows a weaker water transportability in the same condition. It is still hard to give any conclusion on the effect of the oil viscosity and water solubility.

Acknowledge

This thesis is written for the course TPG4920 Master's Thesis, also as a part of my master's degree in Petroleum Engineering with specialization in Reservoir Engineering and Petrophysics at the Norwegian University of Science and Technology (NTNU).

During the year I worked on this thesis, many people helped me, and I wish to express my heartfelt gratitude to them. First, I would like to say thank you to my supervisor, Associate Professor Carl Fredrik Berg (NTNU). He gave me many useful suggestions on topic selection, experiments designing, and practical writing. He also taught me how to write thesis and support me finish the experiments. Second, I would like to say thank you to my co-supervisors Lifei Yan (Utrecht University) and Hossein Mohammad Golestan (NTNU), who helped me much on experiments setting and thesis writing, you are the best partners for me in this year. Also, I would like to say thanks to Roger Overå for his assistance in laboratory.

Finally, thanks for everyone who devoted their help to me. It was so good to meet you at Trondheim!

Wenyu Zhou
Chengdu, China,
30.08.2021

Table of contents

Table of contents i

Lists of Figures ii

Lists of Tables v

1. Introduction 1
2. Background 4
- 2.1. Low salinity water enhanced oil recovery 4
- 2.2. The mechanisms of low salinity water flooding enhanced oil recovery 6
  - 2.2.1. Fine migration 6
  - 2.2.2. Multi Ion Exchange (MIE) 9
  - 2.2.3. pH Increase 10
  - 2.2.4. Double layer expansion (DLOV theory) 11
- 2.3. Emulsification and Osmosis effect in low salinity flooding 14
  - 2.3.1. Osmosis as mechanism for improving oil recovery 14
  - 2.3.2. Spontaneous emulsification as mechanism for improving oil recovery 15

3. Theoretical explanation 26
- 3.1. Liquid membrane 26
- 3.2. Diffusion theory 28

4. Materials and methods 30
- 4.1. Experimental design 30
- 4.2. Microfluidic experiment set-up 32
- 4.3. Pendant drop experiment set-up 37

5. Experimental results 39
- 5.1. Microfluidic experiments results 39
  - 5.1.1. Brine injection without surfactant added 40
  - 5.1.2. Brine injection with surfactant added 43
- 5.2. Light scattering experiments results 49
- 5.3. Pendant drop experiment results 52

6. Discussion 54
- 6.1. LSW Salinity 54
- 6.2. Oil properties 57
- 6.3. Surfactant concentration 59

7. Conclusions and future research advice 61
8. Bibliography 63

List of Figures

Fig. 1: Effects of changes in injection brine composition on recovery of CS crude oil for cyclic water flooding of a CS core 5

Fig. 2: A 25% increase of oil recovery by LSW flooding (around 5000 ppm), from Alaska.... 5

Fig. 3: Proposed low salinity water flooding mechanisms and their relationships with each other 6

Fig. 4: Polar components are absorbed on the rock surface to form a mixed-wet fines 7

Fig. 5: Partial stripping of mixed-wet fines from pore walls during water flooding 7

Fig. 6: Mobilization of trapped oil 7

Fig. 7: SEM characterization of sandstone core samples before and after flooded by different NaCl concentrations, (a) original core sample, (b) core sample flooded by 1.0% NaCl brine, (c) core sample flooded by 0.1% NaCl brine, (d) core sample flooded by 0.01% NaCl brine. 8

Fig. 8: Representation of the diverse adhesion mechanisms occurring between clay surface and crude oil 10

Fig. 9: Proposed mechanism for low salinity EOR effects. Upper: Desorption of basic material. Lower: Desorption of acidic material. The initial pH at reservoir conditions may be in the range of 4 11

Fig. 10: Schema of Electric double layer and the relation with zeta potential 12

Fig. 11: Schema of double layer expansion on clay surface 13

Fig.12: Schematic model of the oil adsorption–desorption process: (a). formation of hydrophobic layers on the rock surface and (b). releasing oil layer when less calcium ions exist when low salinity flooding 13

Fig. 13: In experiments conducted by Sandengen, after the DIW (yellow) flooding, the CaCl2 (blue) expanded and displaced by DIW. Supporting the conclusion of osmosis water transport 14

Fig. 14: Capillaries experiment model set by Fredriksen. LSW is in yellow, red is the oil phase and the white is HSW. Experiment (2) shows a base-line experiment with equal salinity in two sides. 15

Fig. 15: The schematic graph of W/O emulsion and O/W emulsion. Blue is water, brown is oil and yellow stands for the interface with surfactants. 16

Fig. 16: The structure of the micelles for W/O emulsion and O/W emulsion Fig 17

Fig. 17: Schematic representation of surface adsorption of surfactant molecules at the air- water interface and surfactant micelles 17

Fig. 18 Schematic Gibbs free energy profiles of emulsification process driven by external energy and internal energy 19

Fig. 19: Drops of toluene formed by diffusion and stranding mechanism in a toluene brij30 sec-butanol and octanol system 20

Fig. 20: Schematic diagram showing spontaneous emulsification process for a drop of oil in water 20
Fig. 21: Cryo-SEM view of a microdroplet of the microemulsions......................................21
Fig. 22: Schema of spontaneous emulsion in vesicles network structure 22
Fig. 23: Dead-pore structure with HSW and crude oil. Blue, red and black indicate HSW, LSW and crude oil. 22
Fig. 24: (a) Proposed mechanism of spontaneous emulsification. (b) Water diffuses (yellow hatches) into the oil layer while hydrated ions counter diffuses more slowly..........23
Fig. 25 The IFT of the synthetic oil/water with different salinities..24
Fig. 26: Water content-Brine salinity relation diagram 24
Fig. 27: Three configurations of liquid membrane systems: bulk (BLM), supported (immobilized) (SLM or ILM), and emulsion (ELM). F is the source or feed phase, E is the liquid membrane, and R is the receiving phase..26
Fig. 28: The schematic diagram of interaction between oil and water. (a) pure oil under a salinity gradient. (b) surfactants added oil under a salinity gradient. 27
Fig. 29: EOR physical rock network microfluidic chip supplied by Micronit........................32
Fig. 30: Photo of microfluidic system...33
Fig. 31: A schematic picture of the microfluidic system..33
Fig. 32: The microfluidic experiments view under the microscope.......................................34
Fig. 33: Dynamic light scattering device is Zetasizer ZS90 from Malvern Panalytical. (Right)35
Fig. 34: A schematic illustration of the spontaneous emulsification in the DLS chamber......36
Fig. 35: Sketch of the pendant drop experimental apparatus 37
Fig. 36: Drop shape analyzer DSA100E by KRUSS 37
Fig. 37: Images of the isolated HSW area after 1-hour, 24-hour and 48-hour. 41
Fig. 38: Images of the isolated HSW area after 1-hour, 24-hour and 48-hour. 42
Fig. 39: Curves of the variation in HSW area versus observation time for the oil phase without surfactants adding 42
Fig. 40: Images of the isolated LSW/Oil/HSW system for surfactants adding after monitoring from 0 to 80 hours...44
Fig. 41: Images of the reference experiments LSW/Oil/LSW system for surfactants adding. The area increase for connate water is negligible. 43
Fig. 42: Images at 1h, 24h and 48h of the 1% SPAN 80 dodecane with 5% brine as LSW....44
Fig. 43: Images at 1h, 24h and 34h of the 2% SPAN 80 dodecane with 0.2% brine as LSW. 45
Fig. 44: Spontaneous emulsion accumulation was observed after the LSW flooding. (a) picture of the selected LSW/Oil/HSW system; zoomed images giving a close view of the brine-oil interfaces showing the change in emulsion behavior after 24 hours (b), 34 hours (c), and 43 hours (d). 45
Fig. 45: The reference circle needs to fit the reaction interface of HSW as much as it possible.47
Fig. 46: Curves of the variation in HSW area versus observation time for the oil phase with surfactants adding 47
Fig. 47: Dodecane with 1% SPAN 80 contacting with 1700ppm brines. Emulsions deposits after 3 hours and got thicker subsequently. 49
Fig. 48: The emulsion size distribution vis time for heptane and dodecane with 1% SPAN 80 that

contacting with 0.2% and 5% salts brine. 50
Fig. 49: The emulsion size distribution graphs with various salinity brines (0%, 0.2%, 5% and 20%)... 51
Fig. 50: Shape of pendant drop for Dodecane 1% SPAN 80-1700 ppm at different time. (a).0.5 h (b). 1.5 h (c). 8.5 h. The diameter of needle is 0.5 mm.. 53
Fig. 51: The curve of the HSW relative area growth in microfluidic experiments 55
Fig. 52: Relative area curve for Dodecane and Heptane with and without surfactants........... 57
Fig. 53: The emulsion size distribution vis time for heptane and dodecane 58
Fig. 54: HSW relative area curve for dodecane and heptane with 0, 1% and % w/w SPAN 8060

List of Tables

Table 1: The main potential mechanisms of MIE 9
Table 2: Channel information for micro chips 32
Table 3: Microfluidic experiments with SPAN80 to study spontaneous emulsification effect and without SPAN80 to study the osmosis effect (a: experiments with n-heptane; b: experiments with n-dodecane) 39
Table 4: The interfacial tension for pendant water droplets in different oil 52
Table 5: The relative area growth gradient for typical microfluidic experiments 56

1. Introduction

Low salinity water (LSW) flooding is a promising enhanced oil recovery (EOR) method with the strength of low-cost and simplicity. In 1960s, Bernard [1] was the first person who stated that injecting low salinity water (0-1% NaCl brines) into sandstone cores could greatly decrease the core residual oil. After twenty years, low salinity water injection started to get more and more attention from the industry. Lots of field scale and laboratory experiments were operated and confirmed the effect of low salinity water flooding [2] [3] [4]. However, the mechanisms of LSW flooding are not well understood and still are under intense research. For fifty years, the study of mechanisms has focused on the salinity properties, fluid-rock interaction, and oil-water interface reaction. While the mechanisms are still not
fully understood, six of them are considered having the greatest potential:

(1). *Fines migration* [3, 4]
(2). *PH effects* [5]
(3). *multi-component ions exchange* [6, 7]
(4). *Double layer expansion* [8]
(5). *Emulsification* [9-11]
(6). *Osmosis effects* [12, 13]

Several factors like the rock types, oleic and aqueous composition, and the pore structure can highly affect the flooding effect. The previous studies have indicated that after the low salinity water flooding, the wettability of the rock will change to a condition that more favorable for the oil flooding, more water wet [7]. The wettability alteration reduces the flow resistance and thus increase the final oil recovery. Multi-component ions exchange (MIE) and double layer expansion (DLE) are two generally accepted mechanisms to explain this phenomenon.

Advances in imaging technology enable a real-time pore observation of fluids that provides us more direct information on water flooding. In 2014, Mahzari and Sohrabi [14] published their findings about the effect of micro-emulsions, which were generated by crude oil during the contact period with LSW, may result in changes in the oil distribution and oil displacement. Later, other studies indicate that the aggregation of emulsions can change the residual oil distribution and finally improve the oil recovery [10, 11, 15, 16]. Some literature also reported the observation of the osmotic pressure increases over oil film where two sides of the oil film have different salinity brines. Meanwhile, emulsification happened in the oil phase, and the high salinity brine side of the oil showed obvious volume increase [16]. Both the connate water and oil phase may expand during low salinity water flooding, which can change the distribution of oil.

The osmosis effect between connate water and low salinity water over oil films is another mechanism that need to be considered at the fluid-fluid interface. In 2016, Sandegen conducted an experiment that injecting pure toluene as oil phase into microchips and cores, observing connate expansion [12]. Their results showed that the high salinity connate water expanded with nearby low salinity water shrinkage. It indicates that oil phase plays as a semi-permeable membrane which allows water molecules pass through. In 2017, Fredriksen et al. built their own 2-D silicon-wafer microfluidic model to study the osmotic pressure effects, which showed similar results [13]. In our study, we will mainly focus on the fluid interface changes during the emulsification and study the possible mechanisms of the osmosis effect in low salinity water flooding. Considering with uncontrolled factors like microfluidic inner pressure instability caused by valve switching, movement of the observation platform, and weak magnification for microfluidic observations, a sophisticated experimental method needs to be designed. The main body of this master study is performed on a microfluidic system and consists of two parts: Firstly, verifying if the refined oil could act as semi-membrane by osmosis effect during the low salinity water flooding. Secondly, comparing cases with and without adding surfactants in the oil, controlling emulsification around the water-oil interface. By microfluidic experiments and dynamic light scattering analysis, three questions are studied:

(1) Under a salinity gradient condition, can refined oil act as a semipermeable membrane without adding any polar components? And what is the main mechanism for it?
(2) If adding surfactants, can reverse micelles carry water molecules across the oil phase? How does water pass through oil film?
(3) What is the relationship between emulsification and osmosis effect on water transportation during the LSW flooding?

2. Background

To understand the relationship between the industry needs and the experimental work, it is necessary to have a brief introduction of low salinity water and its proposed mechanisms. In this section, we will mainly go through the industry and laboratory studies of low salinity water flooding, discussing the mechanisms but focusing on the main theory of this study -osmosis and emulsification liquid membrane.

2.1. Low salinity water enhanced oil recovery

Enhanced oil recovery (EOR) are methods applied after primary and secondary recovery techniques have exhausted their usefulness [3]. Primary and secondary recovery techniques main rely on the pressure difference between the wellbore with reservoir underground. Enhanced oil recovery methods usually functioned by adding different chemical additives or changing reservoir properties like wettability, permeability, temperature etc.

Low salinity water injection is a relatively new topic in EOR. The first systematic study of low salinity brine flooding was reported by Yildiz and Morrow in 1990 [6]. Many researchers started to focus on this area and study the effect of low salinity water. In 1999, Tang and Morrow tested low salinity with cyclic water flooding on Berea sandstone cores [4]. The core flooding experiment results showed that after repeatedly water flooding, decreasing with injection brine salinity gave significant improvement on the oil recovery. From Fig. 1 we can see that the T1F3, which has the lowest salty concentration, also has the highest recovery factor.

There are also field results supporting the conclusion that LSW can improve oil recovery. Webb et al. in 2003 conducted a series of modified inject log tests, which showed an obvious increase of oil producing after LSW flooding the near well [17]. McGuire also did similar tests in Alaska with single well chemical tracer tests (SWCTT), which confirmed that results could be replicated in a different field [18]. Incremental recoveries of 6 to 12% OOIP were possible in North Slope reservoirs with LSW water flooding. The results indicate that the connate water, injection brines, the crude oil, and the rock all play an essential part in the interactions that determine the sensitivity of oil recovery to brine composition. In recent years, the research on LSW flooding enhanced oil recovery has progressed significantly. Several mechanisms have been discovered by researchers, however no unique mechanism is clearly identified to be the primary cause of the low salinity effect [19].

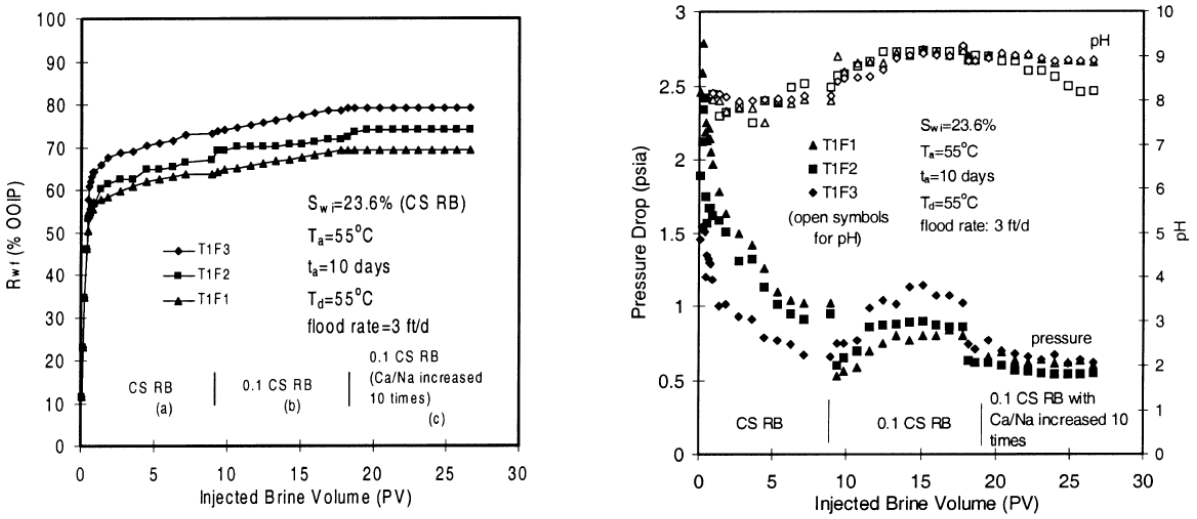

Fig. 1: Effects of changes in injection brine composition on recovery of CS crude oil for cyclic water flooding of a CS core [4]

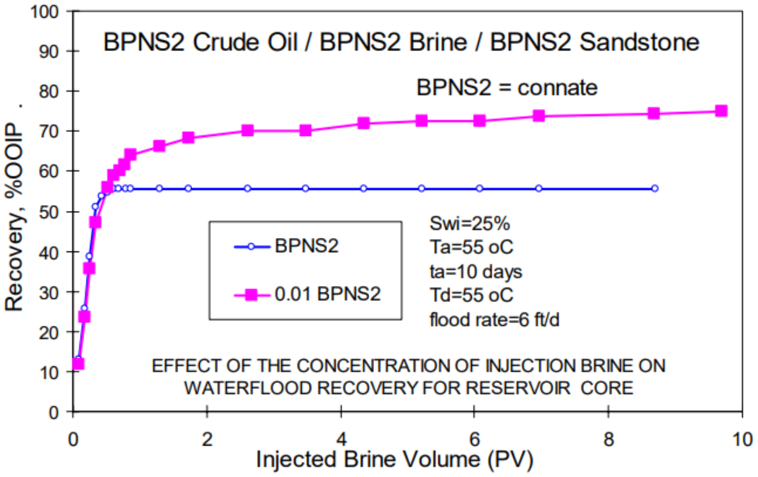

Fig. 2: A 25% increase of oil recovery by LSW flooding (around 5000 ppm), from Alaska. [18]

2.2. The mechanisms of low salinity water flooding enhanced oil recovery

Based on core flood experiments and field research works, many mechanisms have been purported to explain the low salinity water EOR. Because of most of the mechanisms are related to many other mechanisms, a context diagram was made to illustrate these relations as shown in Fig. 3 based on the diagram by Pollen [20]. Based on this diagram, we will go through the main mechanisms in this section.

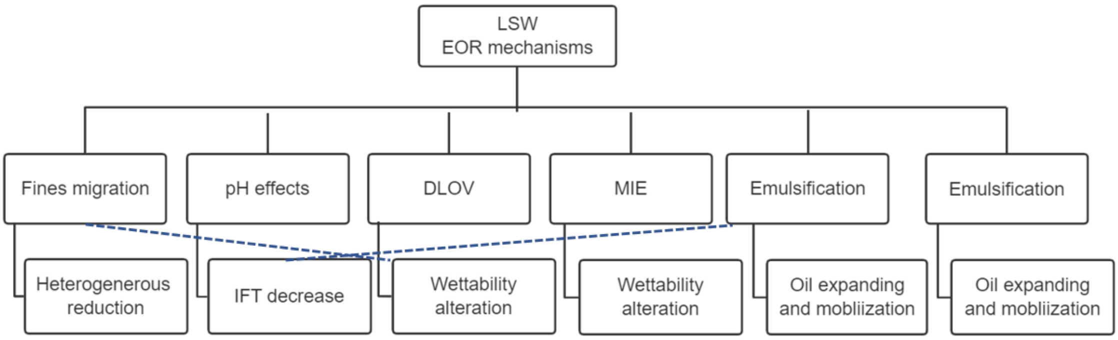
LSW
EOR mechanisms
Fines migration
pH effects
DLOV
MIE
Emulsification
Emulsification
Heterogenerous reduction
IFT decrease
Wettability alteration
Wettability alteration
Oil expanding and mobliization
Oil expanding and mobliization

Fig. 3: Proposed low salinity water flooding mechanisms and their relationships with each other [20]

2.2.1. Fine migration

Fine migration is common in a clay-rich reservoirs. Morrow et al. [4] proposed that additional oil recovery can be caused by a situation with weaker internal bonds in the clay, leading to detachment of clay. Expand surfaces contributes to a more wetness condition during the low salinity water injection. Clay debris, which is got stuck at throat can lead to changes in flow paths and increased oil production. They also reported a reduction of cores permeability after the flooding of low salinity water. Their samples were rich in kaolinite and clay materials. They considered that the expanded detached clay particle work as blocking agent, causing high permeability paths to be blocked, which force the flow into new paths, increasing the sweep efficiency. Especially kaolinite and illite can detach from the rock surface with fresher brines. Injecting low salinity water into a clay-rich reservoir usually have following stages: fines migration, particle swelling, and swelling-induced migration. Fig. 4-6 shows the fins migration process during the LSW flooding.

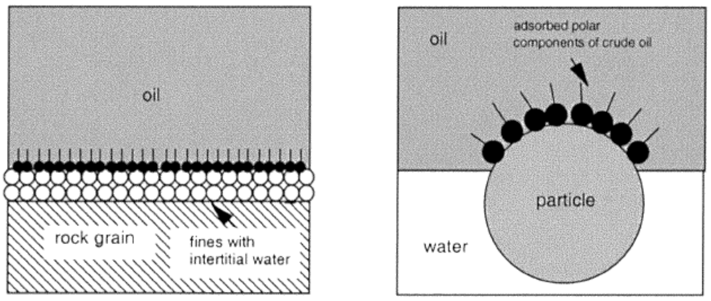
oil
rock grain
fines with
intertitial water
oil
adsorbed polar
components of crude oil
particle
water

adsorption onto potentially mobile fines at low initial water saturation

mobilized particle at oil-water interface

Fig. 4: Polar components are absorbed on the rock surface to form a mixed-wet fines [4]

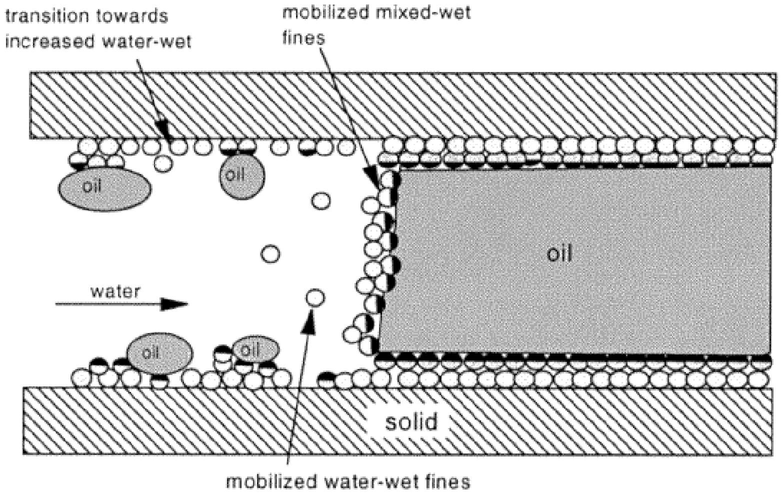
transition towards
increased water-wet
mobilized mixed-wet
fines
oil
oil
oil
water
oil
oil
solid
mobilized water-wet fines

Fig. 5: Partial stripping of mixed-wet fines from pore walls during water flooding [4]

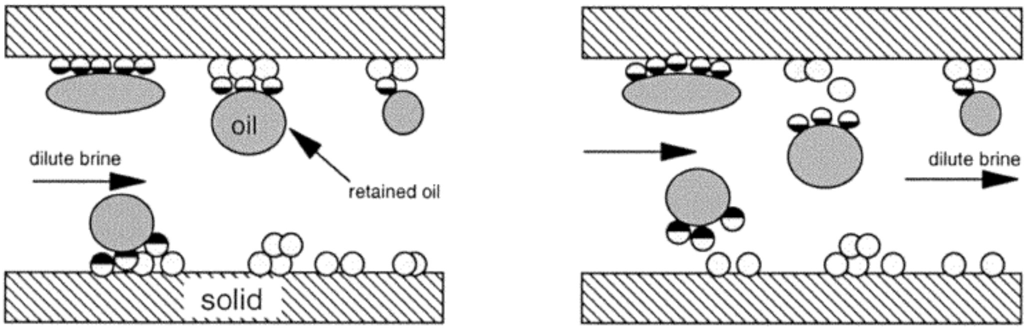
oil
dilute brine
retained oil
solid
dilute brine

retained oil before injection of dilute brine

partial mobilization of residual oil through detachment of fines

Fig. 6: Mobilization of trapped oil [4]

Sheng [21] reported that the low salinity water can make both clay and minerals unstable. In 2018, Alhuraishawy [22] conducted core flooding experiments with different salinity brines injection and SEM observation of core samples before and after the flooding. As Fig. 7a shows, the rock surface of original core sample was very rough where clay particles adhere to the surface. By injecting low salinity brines, the fines detached and migrated from the rock surface. The lower the salinity of brines, the smoother the rock surface. Fig. 7 shows the SEM characterization of sandstone after 3 different salinity brines flooding. His results showed that the LSW flooding will redistribute the flow paths by releasing sand particles and some fine minerals causing a narrowed flow path, which then leads to a better displacement performance.

Some researchers believe that there is no direct evidence indicating a strong connection between fines migration and oil recovery increase. Lager et al. [6] presented that numerous BP low salinity flooding core experiments at reservoir condition showed no fines migration but still had increasing oil recovery. In his conclusion, there is no substantial evidence to show the link between fines migration and oil recovery. Similar results were subsequently identified by other researchers [7, 23] [24]. With the help of imaging, microfluidic can show fines mobilization in real-time. In 2019, W. Song [25] established the microfluidic experiment to directly visualize the pore-scale fines migration during fresh water flooding, including an additional increase in oil recovery.

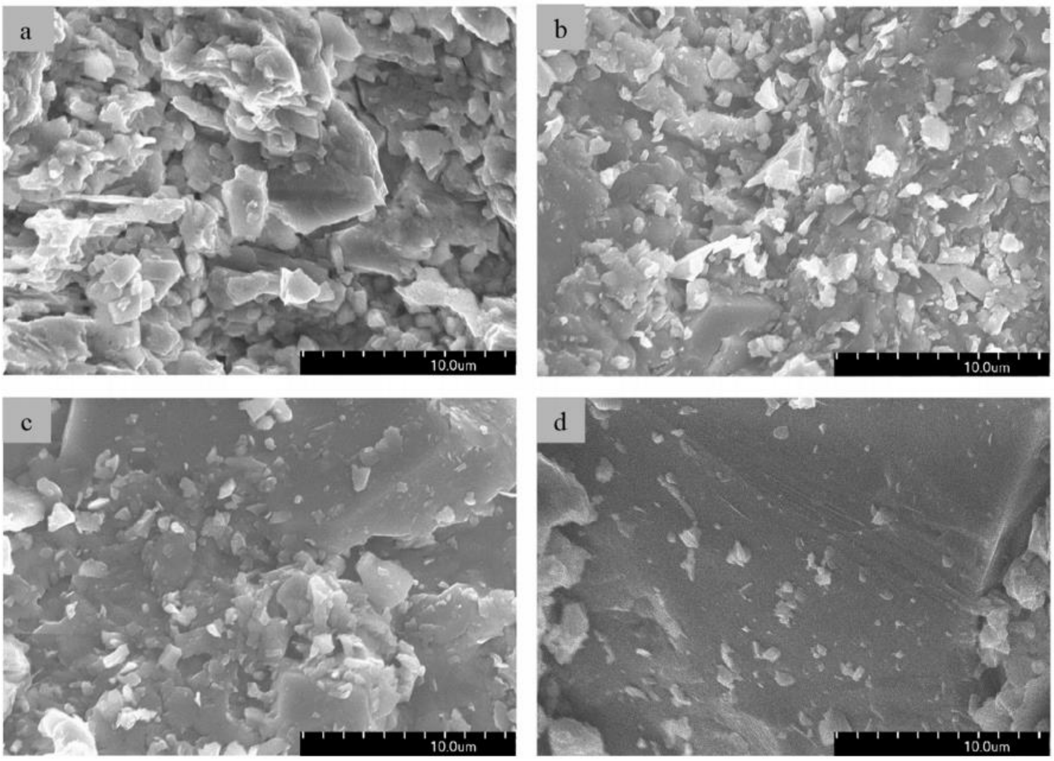

Fig. 7: SEM characterization of sandstone core samples before and after flooded by different NaCl concentrations, (a) original core sample, (b) core sample flooded by 1.0% NaCl brine, (c) core sample flooded by 0.1% NaCl brine, (d) core sample flooded by 0.01% NaCl brine. [22]

2.2.2. Multi Ion Exchange (MIE)

Multicomponent ionic exchange was first suggested by Lager et al. [6] (Fig. 8). He believes that the cation exchange between mineral surface and injecting aqueous phase is the primary mechanism for increased oil recovery during low salinity injection. In the MIE theory, the original oil wet reservoir contains a lot of organo-metallic complexes, which are generated by polar component (resin and asphaltene). After low salinity water flushing over the grain surface, MIE will take place on the both clay and grain surface, increasing the thickness of water and altering the surface more water-wet, then leading to increased oil recovery. By associating field data with laboratory analysis, most of the samples showed decreasing concentration of divalent ions, especially Mg^{2+} and Ca^{2+} changed dramatically [26]. Thus, four possible exchange mechanisms are correlated with MIE occurring in LSW flooding: cation exchange, ligand bonding, cation bridging, and water bridging, as Table 1 shows. Some studies also indicate that Van der Waals interactions, ligand exchange and cation bridging are the dominant adsorption mechanisms [6].

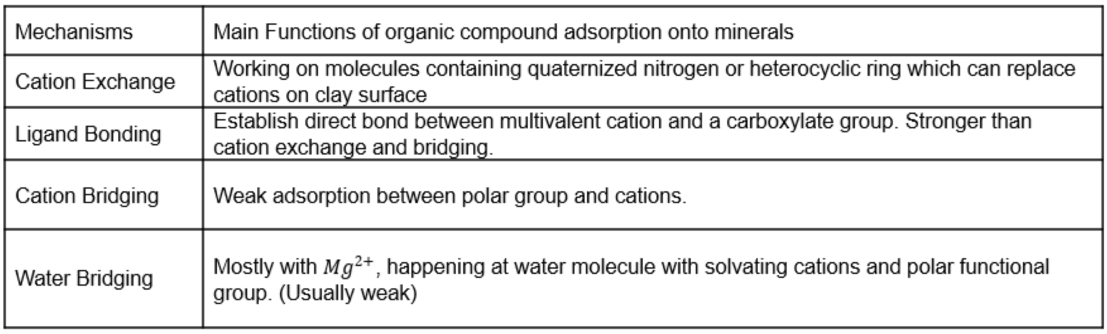

Mechanisms	Main Functions of organic compound adsorption onto minerals
Cation Exchange	Working on molecules containing quaternized nitrogen or heterocyclic ring which can replace cations on clay surface
Ligand Bonding	Establish direct bond between multivalent cation and a carboxylate group. Stronger than cation exchange and bridging.
Cation Bridging	Weak adsorption between polar group and cations.
Water Bridging	Mostly with Mg^{2+}, happening at water molecule with solvating cations and polar functional group. (Usually weak)

Table 1: The main potential mechanisms of MIE [6]

During the LSW flooding, cation exchange usually happened when molecules containing quaternized nitrogen or heterocyclic ring alter the metal cations which initially bound to clay surface. Ligand bonding occurs between a multivalent cation and a carboxylate group, formatting stronger bonds than cation bridging and cation exchange bonds and leading to the detachment of organo-metallic complexes from the mineral surface, especially in Mg^{2+} solvated water. All four mechanisms of MIE are illustrated as Fig. 8 shown. In 2011, T. Austad [7] suggested that the MIE may be linked with the change in the concentration of Mg^{2+}. However, it is not completely caused by MIE as the increase of pH around clay surface can generate $\mathrm{Mg(OH)_2}$ during this period. Due to the generation of $\mathrm{Mg(OH)_2}$, local alkalinity can also decrease and may impact the desorption of organic material from the clay surface, which have a similar phenomenon as MIE. Meanwhile, Austad also discussed the works of the polar component in the crude oil. The adsorption of basic and acidic material which are important compositions of the polar component attached onto clay minerals is very sensitive to changes in pH. An increase in pH is needed to remove some of the adsorbed organic material on the clay surface. We will discuss this detailly in the next section. [7]

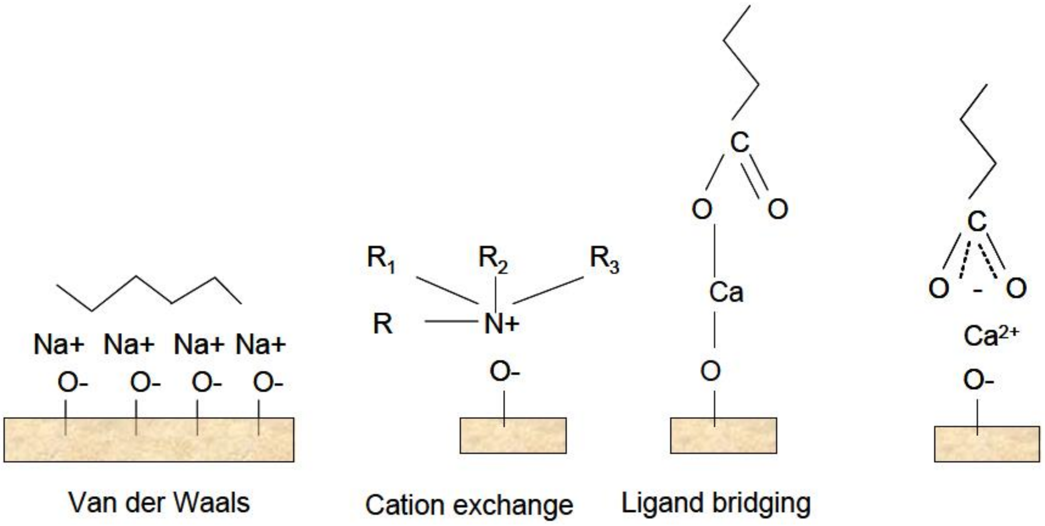

Fig. 8: Representation of the diverse adhesion mechanisms occurring between clay surface and crude oil [6]

2.2.3. pH Increase

PH increase has been reported in some early research on low salinity water flooding. During core flooding experiments, Tang and Morrow [3] observed a production of the fine particles and displaced water pH showed an increase. T. Austad [7] emphasized that the local pH around clay surfaces may domain the effects of low salinity enhanced oil recovery. The chemical equilibrium is established by both basic and acidic organic materials absorbing onto the clay. So, three assumptions are established for enhanced oil recovery by LSW through such chemical mechanisms:

1. *Appropriate clay properties and enough amount present in the rock.*
2. *Polar components in the crude oil, both acidic and basic.*
3. *Inorganic cations present in formation water, especially* Ca^{2+}.

The clay could act as a cation exchanger on its surface area. When the low salinity water flooded inside the reservoir, the equilibrium associated with the brine-rock interaction is disturbed, which is usually Ca^{2+} and Mg^{2+}. The protons from the water will absorb onto the clay to offset the lack of charge. In the end, one hydroxyl ion will release into the water which can cause an increase of pH. Except the cations, some acidic and basic material can also have the similar reaction as shown below.

$$Clay - Ca^{2+} + H_2O = Clay - H^+ + Ca^{2+} + OH^-$$

$$Clay - RCOOH + OH^- = Clay + RCOO^- + H_2O$$

$$Clay - NHR_3^+ + H_2O = Clay + R_3N + H_2O$$

The suggested mechanism is schematically illustrated in Fig. 9 for adsorbed basic and acidic material. Both adsorbed basic and acidic material are detached from the clay surface, causing a wettability change to more water wet condition [27]. Additionally, for water-oil interaction, the Ph increase will also accelerate the emulsification and help to stabilize the water in oil emulsion [28]. Generally, increasing pH can be considered as both a root mechanism and a result caused by ion exchange.

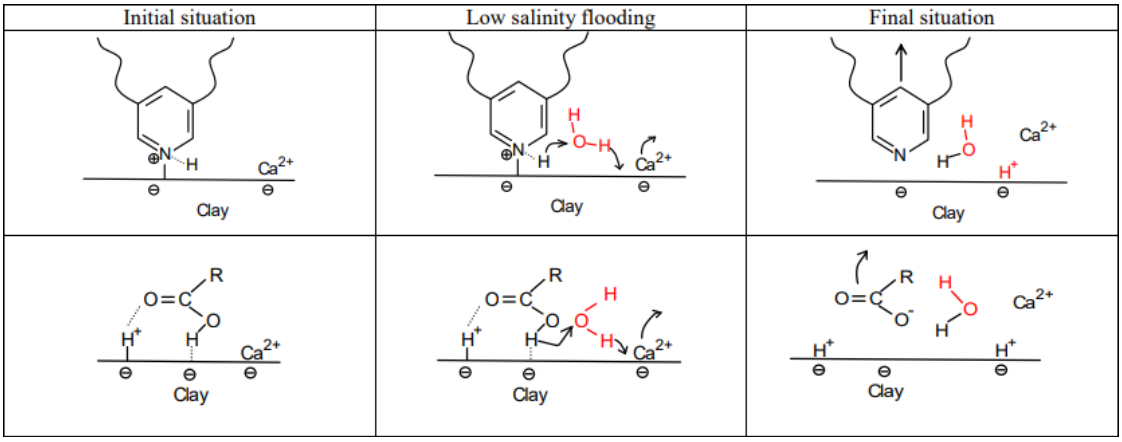

Fig. 9: Proposed mechanism for low salinity EOR effects. Upper: Desorption of basic material. Lower: Desorption of acidic material. The initial pH at reservoir conditions may be in the range of 4

2.2.4. Double layer expansion (DLOV theory)

Winsauer and Mccardell [29] first used excess double layer to explain different conductivity in reservoir rock. The double layer theory is a theory of colloidal dispersion stability where the zeta potential can be used to evaluate the ionic repulsion created by the closing particles. The zeta potential is the electrical potential at the slipping plane, as Fig. 10 illustrated. The double layer combines with the effects of van der Waals attraction and the electrostatic repulsion. The total potential energy is described as the sum of the attraction potential and the repulsion potential. In this system, the Van der Walls force is only a function of distance. For electrostatic repulsion, it can be represented by zeta potential. The electrostatic repulsion force usually works on maintaining the colloid stability of the water oil system. Usually, if two particles get very close to each other, the attracting could dominate the process and make them contact. As the distance increases, the potential energy, described as the combination of attraction potential and the repulsion potential, may find a thermodynamic equilibrium state (primary minimum). If the energy barrier was higher than primary minimum but not high enough to make particles detach completely, particles may stay at the second minimum. There is a high energy gap for the detachment stage [30]. Due to the change of brine salinity, electrostatic repulsion can fluctuate a lot, which may lead to instability in the water micro-environment between the oil and the clay surface. The excess double layer conductivity is depending on the specific ions in the electrolyte and the total salt concentration. As the concentration of salts in water gets lower, the surface charge of clays can change to negative, which make the repulsive forces exceed the binding forces via the multivalent cation bridges, causing the oil particles to be desorbed from the clay surfaces [8]

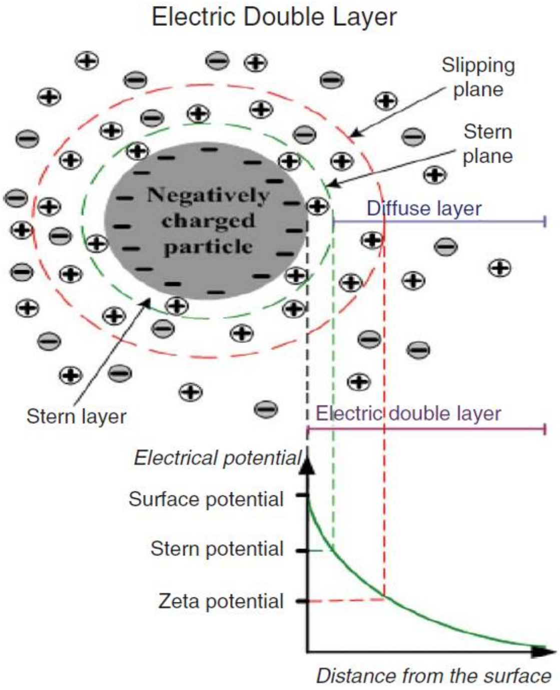
Electric Double Layer
Slipping plane
Stern plane
Negatively charged particle
Diffuse layer
Stern layer
Electric double layer
Electrical potential
Surface potential
Stern potential
Zeta potential
Distance from the surface

Fig. 10: Schema of Electric double layer and the relation with zeta potential [31]

Ligthelm et al. [8] indicated that wettability alternation by double layer extension is the primary mechanism of LSW injection. For high salinity brine, a relatively thin double layer film exists between the oil droplet and clay surface, making it act as oil wet. After the low salinity water flooding, the film between low salinity water and rock will expand, making the rock surface more water wet. Fig. 11 shows the difference after the low salinity water flooding. In real reservoir conditions, both simulations and laboratory experiments have verified that the electrovalence plays an important role in water film thickness [8] [31]. The thickness of the double layer is very sensitive to electrovalence. Comparing with water only added sodium chloride, injecting water with divalent cations like calcium ions, magnesium ions yields less oil production [8]. Based on the FESAM (Field Emission Scanning Electron Microscopy) and the chemical analysis of the core flooding samples, Yang [32] indicated that the calcium bridges are much stronger and more effective than sodium bridges, and van der Waals forces to help organic materials adsorb onto minerals. Fig. 12 shows this process.

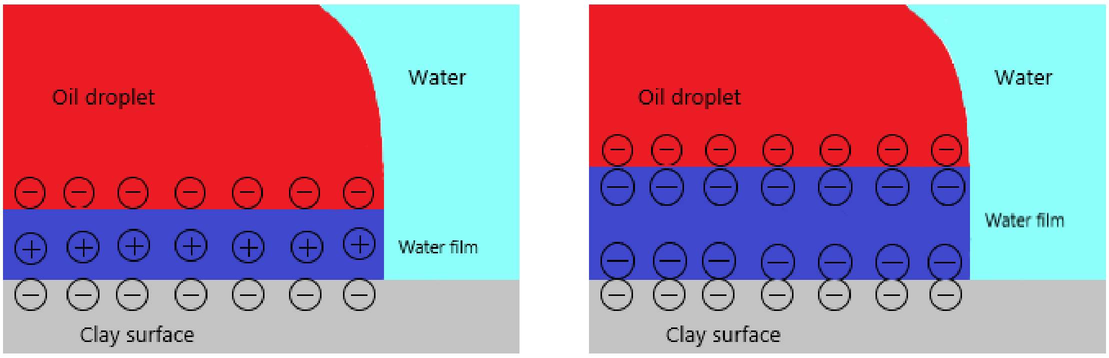
Oil droplet
Water
Water film
Clay surface
Oil droplet
Water
Water film
Clay surface

Fig. 11: Schema of double layer expansion on clay surface

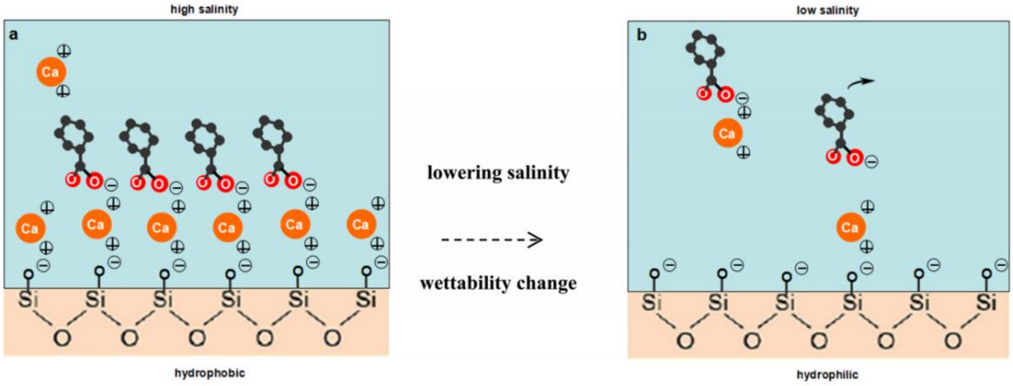
high salinity
a
Ca
Si
O
hydrophobic
lowering salinity
wettability change
low salinity
b
hydrophilic

Fig. 12: Schematic model of the oil adsorption−desorption process: (a). formation of hydrophobic layers on the rock surface and (b). releasing oil layer when less calcium ions exist when low salinity flooding [32]

It is noted that both DLOV and MIE as mechanisms for LSW EOR are based on the fact of wettability alteration. The wettability alteration sometimes is considered as an accompanying effect of the low salinity water effect, not the cause of LSW effects [7, 31]. The coexistence of DLOV and MIE effect on the wettability alteration is not contradictory but which one affects the most is still uncertain. After dozen years of study, we found that the mechanisms of LSW flooding enhanced oil recovery are very complicated. Therefore, the low salinity effect is a result of different mechanisms acting together, each with its own contribution.

Note that all four mechanisms presented above are related to the fluid-rock interaction in rock systems. There is still no certain conclusion on LSW enhanced oil recovery mechanism. Lately, the effect of the fluid-fluid interaction has received more attention from academia. Spontaneous emulsification and osmosis are two potential mechanisms in LSW flooding. The process and the mechanisms for them are still unclear. In the following section, a brief introduction of the spontaneous emulsification and osmosis will be given.

2.3. Emulsification and Osmosis effect in low salinity flooding

2.3.1. Osmosis as mechanism for improving oil recovery

Based on previous emulsification studies, Sandengen published his study about the osmosis effect in low salinity water injection in 2013 [33]. Osmosis is a thermodynamic driving force for water transport caused by a difference in chemical potential between two aqueous solutions separated by a semi-permeable membrane [13]. The results by Sandengen showed that the high salinity connate water expanded with nearby low salinity water shrinkage. It indicates that the oil phase acts as a semi-permeable membrane which only allows water molecules to pass through. In Sandengen's studies, both 2D microfluidic model and core X-ray scans were used to observe the expansion of connate water. In an oil wet environment, the high salinity connate water expands and pushes the oil film between HSW and LSW. After the LSW injection, the oil film contacted by LSW gradually appeared darker. Observing at a higher magnification, the darker area showed agglomerates of small bubbles. These small bubbles were not affected by pressure changes, which indicates that they are water emulsions. In the study by Emadi and Sohrabi [34], they described these water emulsion as 'micro-dispersions' to distinguish them from micro-emulsions. It is emphasized that they used crude oil, not synthetic oil. To avoid the interference of the micro dispersions, heating and cooling were introduced to provoke micro-emulsions on both sides of the oil film in the microfluidic experiments. The purpose of generating emulsion was to create an equal concentration of micro emulsion on both sides of the oil film. The case with assumed constant concentration of emulsions showed the same result as the previous experiments. This indicated that osmosis is an independent mechanism during low salinity water injection.

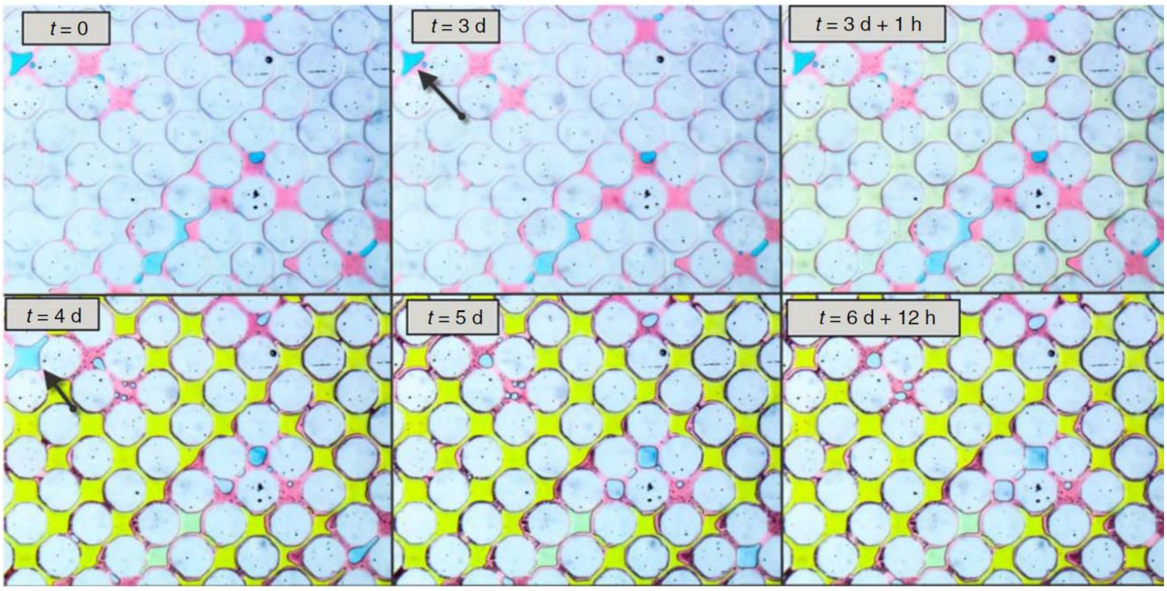

Fig. 13: In experiments conducted by Sandengen, after the DIW (yellow) flooding, the $CaCl_2$ (blue) expanded and displaced by DIW. Supporting the conclusion of osmosis water transport [12]

In 2017, Fredriksen repeated the osmosis experiment by using capillaries, giving similar results as Sandengen [13]. Oil-wet polytetrafluoroethylene (PTFE) tubes was used. These were injected with LSW, toluene and HSW sequentially. After 20 days, almost all the LSW (yellow) was transported into the HSW (white), as shown in Fig. 14 (1). Sample without salinity gradient has no water transport for 20 days, as shown in Fig. 14 (2). Lifei [16], Naeem [35] also conducted similar capillary experiments, supporting the conclusions that both crude oil and synthetic gives oil osmotic water transport. However, in some realistic situations for LSW injection, osmosis usually works alongside other mechanisms such as, spontaneous emulsification and wettability alteration, which are also highly affected by the water salinity. The effect of osmotic water transport in EOR process is therefore hard to quantify.

It should be noted that the synthetic oil used by Sandengen and Fredriksen was toluene, which has a very high water solubility, similar with the water content in crude oil. However, one difference between synthetic oil and the crude oil is that the existence of the polar component, which can act as the surfactants and form emulsions. It is still unclear that how much water is diffused into the oil film due to the osmosis or the emulsification. To study the osmosis effect during the LSW flooding, choosing the oil with a high water solubility may overestimate the water diffusion effect.

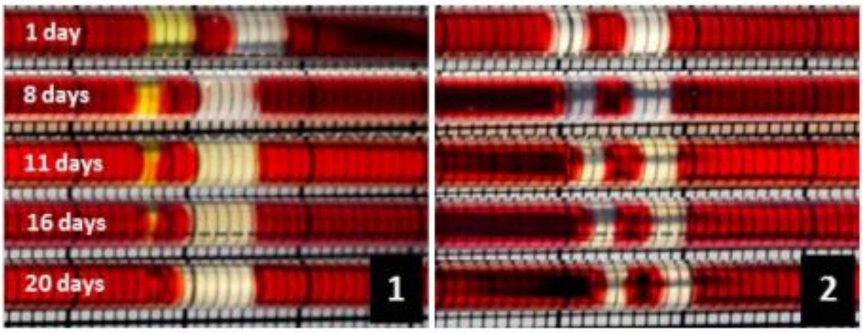

Fig. 14: Capillaries experiment model set by Fredriksen. LSW is in yellow, red is the oil phase and the white is HSW. Experiment (2) shows a base-line experiment with equal salinity in two sides. [13]

2.3.2. Spontaneous emulsification as mechanism for improving oil recovery

An emulsion has been defined as a thermodynamically unstable heterogeneous system of two immiscible liquids where one is dispersed in the other [36]. In petroleum industry, the crude oil mixing with gas or water are the main objects to be studied on. Emulsion plays a vital role in many aspects, including drilling mud, enhanced oil recovery, acid fracturing and separation etc. In enhanced oil recovery, emulsions are usually formed by crude oil, water, and surfactants. These surfactants are usually some polar components in crude oil. Water in oil (W/O) and oil in water (O/W) emulsions, even water in oil in water (W/O/W) and oil in water in oil emulsion (O/W/O), can be observed during the water flooding, however the most familiar ones are the first two emulsions [37]. As shown in Fig 15 (a) that the W/O system appears when water droplets play as a dispersed phase and mixing in the continuous oil phase. The O/W emulsions are inverted, as shown in Fig 15 (b). When the reservoir system is not static, during water flooding, the emulsions are always breaking up and re-forming, which leads to a very complicated system. The W/O emulsion is usually recognized at the down-hole or in the reservoir at early stage of flooding as the flow stream then consists of more hydrocarbon than water. At the late stage of water flooding, the water takes up more volume which leads to a O/W emulsion.

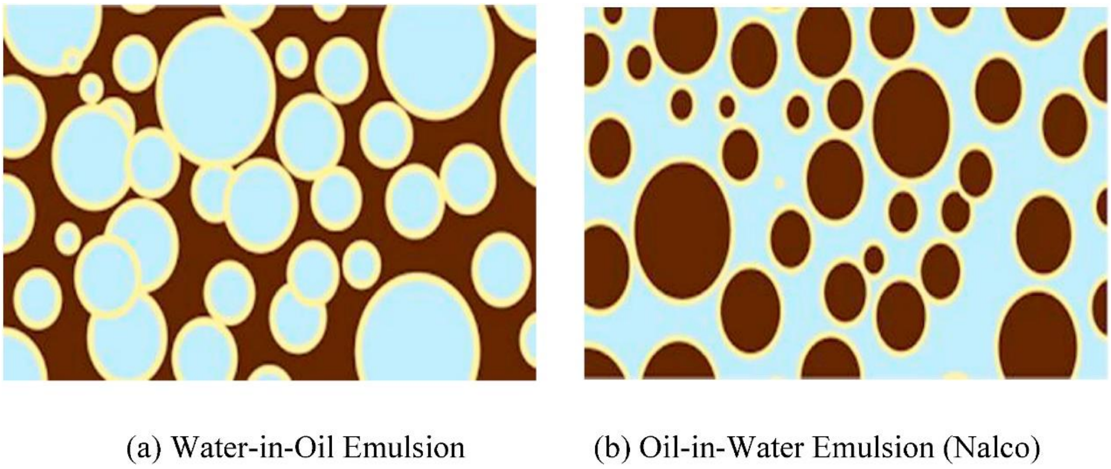
(a) Water-in-Oil Emulsion (b) Oil-in-Water Emulsion (Nalco)

Fig. 15: The schematic graph of W/O emulsion and O/W emulsion. Blue is water, brown is oil and yellow stands for the interface with surfactants. [38]

Emulsification is defined as the process of emulsions formation. In oil reservoir, the emulsification is a complicated physical and chemical process influenced by several factors, such as reservoir temperature and pressure, rock wettability, fluid properties, and pore structure. Under different circumstances, the emulsions have various behaviors on rheology and fluid-rock interaction, which can enable enhanced oil recovery on purpose. Surfactants EOR for example, is one of the most important application of EOR by emulsification. Surfactant flooding is a EOR technique used for mobilizing residual oil trapped in the reservoir. The surfactants can highly reduce the IFT between the oil and brine, alter the rock wettability of the porous medium, which can contribute to mobilizing residual oil.

Emulsions of any significant stability should contain two immiscible fluids, and at least one emulsifying agent. The emulsifying agent, usually known as surface-active agent or surfactant, groups on the two fluids interface to reduce the interfacial tension. Surfactants are characterized with two functional groups, one hydrophilic and one hydrophobic. The hydrophilic group is water soluble and the hydrophobic is oil soluble. The energetically most favorable orientation for surfactants molecules is on the oil water interface, so that each side of the surfactant is placed towards the greatest affinity to minimize the energy. Because of this arrangement need some time to establish itself, the process of accumulation and arrangement is dynamically. Many factors can affect this process, such as salinity, ions properties, temperature, and the fluid properties. When the concentration of surfactants around the interface is above the critical concentration needed to cover the fluid-fluid interface, also known as CMC (critical micelle concentration), the surfactants molecules can assemble the insoluble phase molecules and create the micelles in the soluble phase.

The micelles structure for O/W and W/O emulsion are shown as Fig. 16. The surfactant monomer usually exists on the fluid-fluid interface where the surfactant molecules show the consistent posture that the hydrophilic side towards water and hydrophobic side towards oil. Surfactant multimer is also called emulsion micellar. Meanwhile, the surfactant molecules can have a kinetic exchange between monomer and multimer at equilibrium. In general, the process of emulsification is referred to as a dynamic process. Fig. 17 shows this process schematically. In crude oil system, two immiscible fluids can be water/oil and gas/oil. For emulsifier, evidence indicates that the asphaltenes and the resins contents in the crude oil are the effective components for emulsion formation [39-41]. Fingas in 2014 [41] reported that the asphaltenes are the content in the crude oil that keeps emulsions stable, while the resins help the asphaltenes to be soluble in the oil phase.

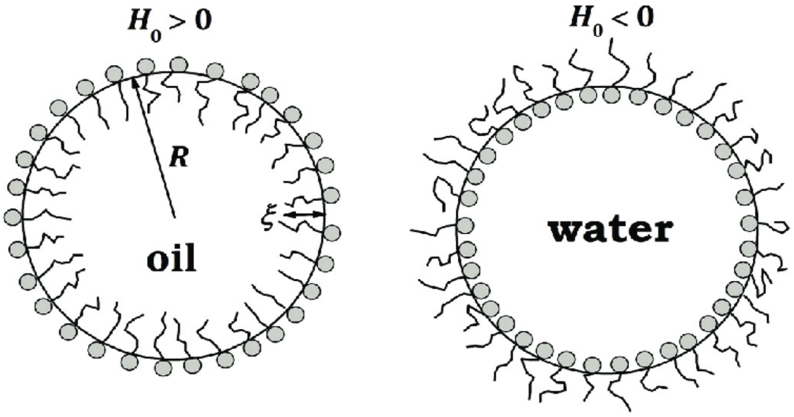

Fig. 16: The structure of the micelles for W/O emulsion and O/W emulsion Fig [42]

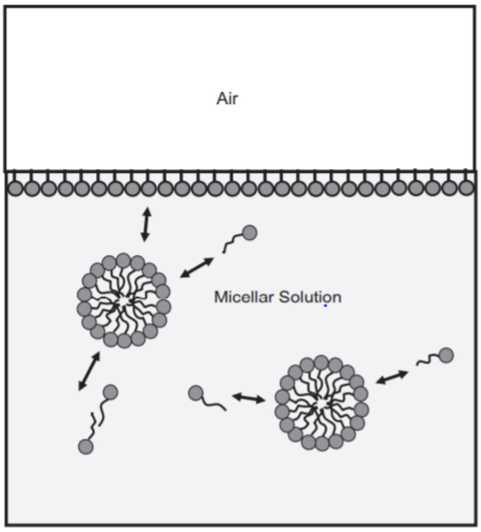

Fig. 17: Schematic representation of surface adsorption of surfactant molecules at the air- water interface and surfactant micelles [43]

Emulsions are very complicated systems. Below is a list of factors that emulsions are influenced, given by the Kanicky [44], which can help us evaluate emulsion formation.

- Chemical composition (molecular structure and concentration) of oil
- Chemical composition (types and concentration of salts present) of water
- Chemical composition (nonionic, anionic, cationic, zwitterionic and polymeric) and concentration of surfactants
- Structure and concentration of cosurfactants
- Number and types of finely divided particles present
- Temperature and pressure of the system
- Order of mixing of emulsion constituents
- Energy input

Spontaneous emulsification occurs in the oil phase during the low salinity injection and is considered an important factor for enhancing oil recovery [19]. Many researchers reported direct observation of emulsion generation with low salinity injection in microfluidic system. They suggested that the amount of water in oil emulsions can be used to evaluate the effects of the water injection [13, 34, 45]. In a developing reservoir, residual oil and high salinity water usually co-distribute in the swept region after primary displacement. Increasing water in oil emulsions causes expansion of the oil phase, which leads to mobilization of oil [13]. Emulsions also can be considered as a flow path, allowing water to be transported through oil films into connate water. This phenomenon is also called emulsion liquid membrane. However, the effects of emulsions on water transportation are still unclear.

To understand the emulsification during low salinity water injection, we need a clear definition of spontaneous emulsification. The phenomenon of spontaneous emulsification can be described as self-emulsification, which is defined as the process of emulsions droplets formed by two immiscible liquids that out of in equilibrium due to external energy input. It can be explained by the schematic graphs shown in Fig. 18. The Gibbs free energy equation is defined as:

$$\Delta G = \gamma \Delta A - T \Delta S$$

where the $\gamma \Delta A$ is the interface initial energy and $T \Delta S$ is the entropy of the dispersion. For a system in equilibrium, the entropy of the dispersion is positive and much lower than the interfacial energy, which will lead to a positive free energy, as Fig. 18 (a) shows. So that the external energy is required to generate emulsions. As indicated in Fig. 18 (b) for spontaneous emulsification, the free energy in the current state is higher than for forming emulsions, so emulsion generation gives the ΔG<0, emulsion can occur spontaneously [46].

In a study by Lopez-Montilla and Herrera-Morales, they discussed many mechanisms of spontaneous emulsification [47]. Among them, three mechanisms are related to our case: (1) interfacial turbulence (2) diffusion and stranding and (3) negative interfacial tension.

(a) External energy

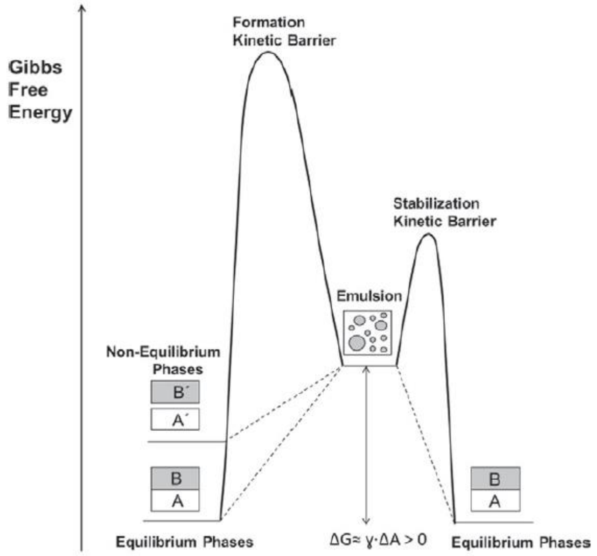
Gibbs Free Energy
Formation Kinetic Barrier
Stabilization Kinetic Barrier
Emulsion
Non-Equilibrium Phases
B´
A´
B
A
B
A
Equilibrium Phases
ΔG≈ γ·ΔA > 0
Equilibrium Phases

(b) Internal energy

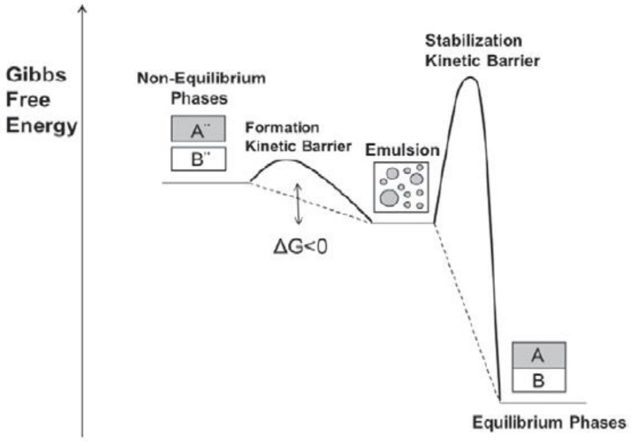
Gibbs Free Energy
Non-Equilibrium Phases
A''
B''
Formation Kinetic Barrier
Emulsion
Stabilization Kinetic Barrier
ΔG<0
A
B
Equilibrium Phases

Fig. 18 Schematic Gibbs free energy profiles of emulsification process driven by external energy and internal energy [46]

Interfacial turbulence: When two fluids are contacting each other with no external additive energy, the interface between them can start to develop unsteady motions, which may lead some fluid molecules to diffuse through the interface. These molecules can be stabilized by other forces, like gravity or osmotic pressure [47]. However, in our case, the interfacial turbulence usually acts in a complex situation, where extra energy from the movement of injected low salinity water can lead to huge interface instability too. The pure interfacial turbulence mechanism is not considered as the main reason for spontaneous emulsification during EOR.

Diffusion and stranding: This mechanism requires the occurrence of droplets with a high value of interfacial tension in one fluid and a low value of interfacial tension in the other fluid. In simple terms, emulsions are created by a third component partly miscible with two immiscible fluids. Fig. 19 shows the direct observation by microscope of diffusion droplets of toluene in a water phase. An example showed at Fig. 18 of this mechanism occurs with an ethyl alcohol-toluene-water system, as presented by Lopez-Montilla [47].

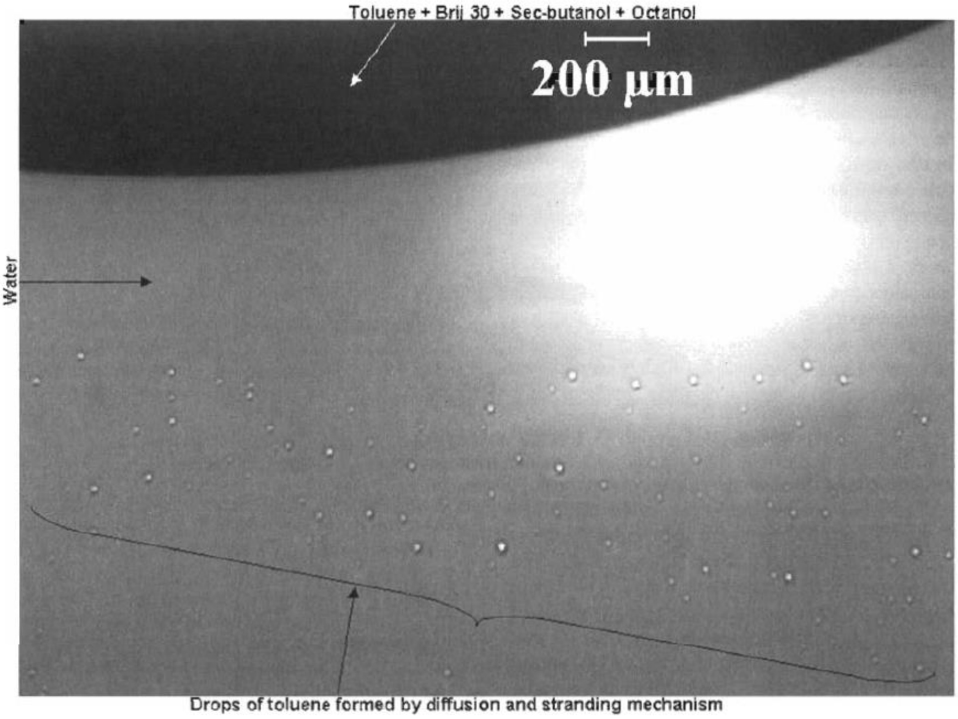
Toluene + Brij 30 + Sec-butanol + Octanol
200 µm
Water
Drops of toluene formed by diffusion and stranding mechanism

Fig. 19: Drops of toluene formed by diffusion and stranding mechanism in a toluene brij30 sec-butanol and octanol system [47]

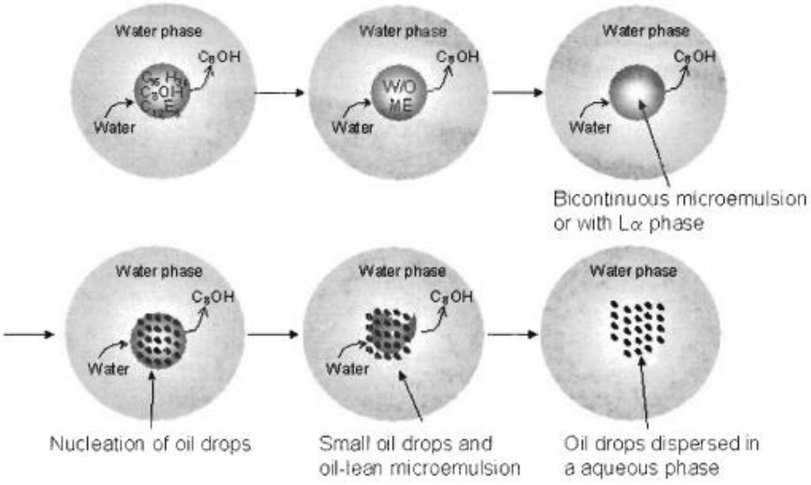
Water phase
C8OH
C16H33
C8OH
C12E4
Water
Water phase
C8OH
W/O
ME
Water
Water phase
C8OH
Water
Bicontinuous microemulsion
or with Lα phase
Water phase
C8OH
Water
Nucleation of oil drops
Water phase
C8OH
Water
Small oil drops and
oil-lean microemulsion
Water phase
Oil drops dispersed in
a aqueous phase

Fig. 20: Schematic diagram showing spontaneous emulsification process for a drop of oil in water

Negative interfacial tension: The last mechanism is negative interfacial tension. It was shown that the negative interfacial tension can occur in the certain water-oil-surfactants systems. If we put toluene containing cetyl alcohol on the top of an aqueous solutions of sodium dodecyl sulfate, the spontaneous emulsification will take place when the concentration of alcohol is beyond a specific concentration limit. The total interfacial tensions of the whole system will have a very low value, it could even be negative [47]. In recent studies, people believe that negative interfacial tension is not the main factor causing spontaneous emulsification [46]. The negative interfacial tension is usually altered by low interfacial tension, mainly caused by sufficient surfactants around the interface that extra surface area is created by diffusion fluids and surfactants. The extreme low interfacial tension allows more solvents into the solution. Otherwise, low interfacial tension is still an essential prerequisite to generate emulsions [48].

As we mentioned above, with the help of surfactants to lower the interfacial tension, this nonequilibrium system can lead to injection water diffuse into the oil phase and create microemulsions. These microemulsions in the oil phase are nano to micrometer scale. When low salinity water contacts with oil, emulsions are generated and assembled around the interface, shaping microemulsions with diameters from 1 to 100 micrometers. Large droplets are usually connecting with small droplets, which make a net structure, as Fig 21 shows [49]. The size of droplets or vesicles are affected by temperature, pressure, the concentration of surfactants and solvents, etc. Besides droplets, the environment is still oleic, and the mobility of oil molecules will decrease. The structure showed in Fig. 21 and Fig. 22 can give us a rough feeling of emulsion structure [50] [51].

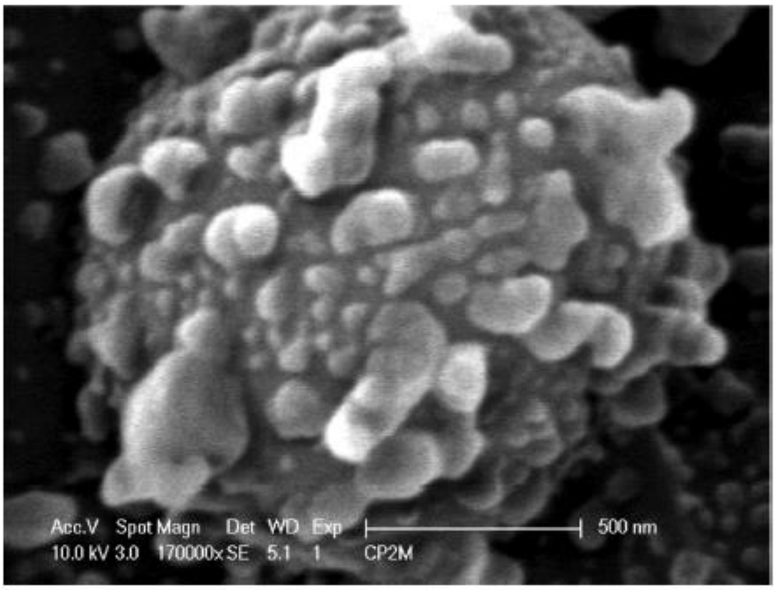

Fig. 21: Cryo-SEM view of a microdroplet of the microemulsions [49]

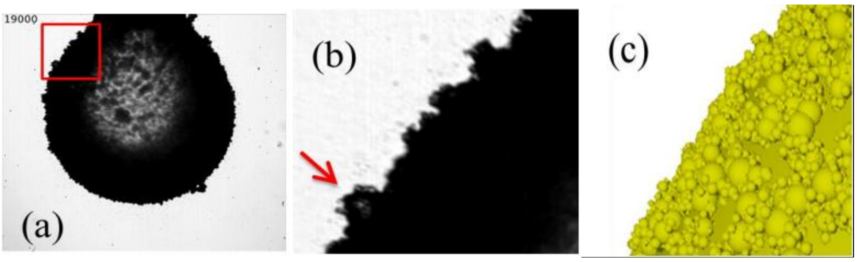

Fig. 22: Schema of spontaneous emulsion in vesicles network structure [49]

After normal water flooding, there is still remaining oil trapped in dead-end pores [52]. In this situation,placement could be a stack of high salinity water in the end of the dead-end pore, covered by trapped oil, and then flowing water. The emulsions are generated at the oil phase in the middle of the system. Fig. 23 gives a good example of this structure [53]. Flowing injection water bring the needed free kinetic energy continuously, which create a nonequilibrium system. As we have already discussed the spontaneous emulsification with oil and water, the emulsion system in LSW-Oil-HSW structure would be our target to study. In a recent study, a simplified model was presented by Aldousary and Kovscek as Fig. 24 (a) shown [10]. For the initial situation, oil is equilibrated with the connate water. As far as we know, the amount of hydrated ions and water molecules that can be dissolved into the oil phase with very limited content in contacting. For instance, in 25 °C the water solubility in n-dodecane is around 65 ppm, and in 40 °C it is 127 ppm. Aldousary and Kovscek [10] pointed that the diffusion coefficient of water molecules in oil is two orders magnitude higher than the hydrated ions. When the surfactants occupying the interface, water molecules are easier to pass through the interface than hydrated ions. The concentration of these contents in oil are also affected by the oil properties [54]. The interfacial tension(IFT) gradually increases with the increase of salinity [55]. The relation curve is shown in Fig.25.

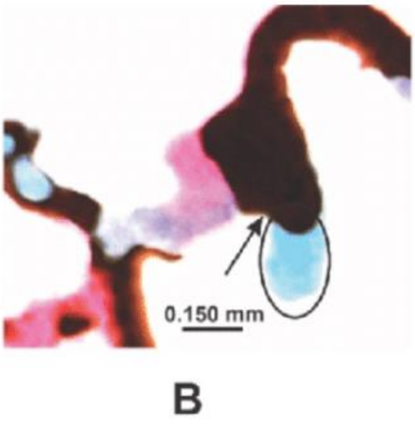

Fig. 23: Dead-pore structure with HSW and crude oil. Blue, red and black indicate HSW, LSW and crude oil. [53].

The amount of water diffusing into the oil phase is highly influenced by the temperature, water salinity and oil properties. At the high salinity water side, the IFT is relatively high, contributing to less water dissolving into the oil and restricting the size of the emulsion droplets [55]. Fig. 26

shows the water contents in oil for water with different salinity. As the brine concentration higher than the threshold limitation, emulsions will not generate around the interface and the system will be not in equilibrium.

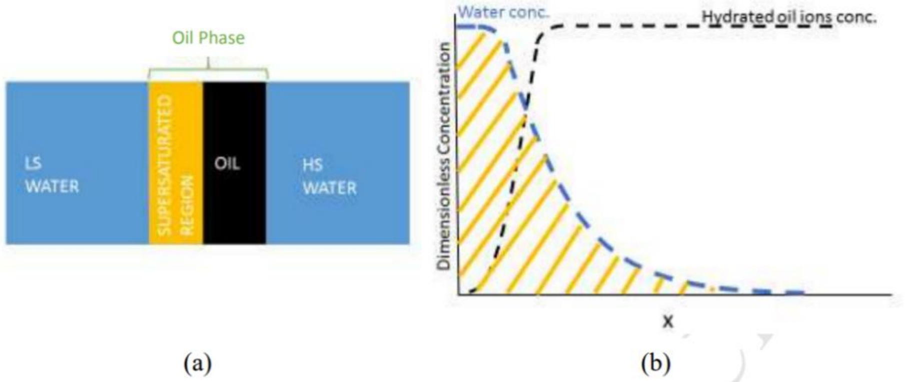

Fig. 24: (a) Proposed mechanism of spontaneous emulsification. (b) Water diffuses (yellow hatches) into the oil layer while hydrated ions counter diffuses more slowly.

After injecting the low salinity water, a super-saturation zone will form at the low salinity water-oil interface, as Fig. 24 (a) shown. A super-saturation zone means that in a region of oil, the water contents far beyond the water solubility. In general, the creation of a super-saturation zone is a process of spontaneous emulsification. When low salinity water approaches the oil interface, the polar components, which is regarded as the surfactants in crude oil, will be attracted to the interface. Considering oil components like alkane, benzene compound, hydrophilic parts favor water molecules and embeds with them on the interface, while the hydrophobic part is affected towards the oleic phase. Because the intermolecular forces between surfactant and water molecules are much lower than oil/water molecules, the surface tension will decrease [56]. When the concentration of surfactants around the interface is above the critical micelles concentration (CMC), reverse micelles will generate by diffused water molecules and dissociative polar components, shaping of emulsion droplets. As the concentration of emulsion increases, the nucleated emulsion droplets may remain as a group and coalesce to larger droplets based on the balance between Gibbs free energy and entropic limitations [57]. However, the size of these reverse micelles is highly dependent on the brine salinity, oil properties, and surfactants [54]. At the high salinity water interface, there is no obvious emulsification. From the study by Perles [58], the increasing ionic strength may cause more asphaltene and resin molecules to adsorb at the interface, forming more compact and rigid films. The repulsion between the charges of adsorbed molecules can cause the destruction of micelles interface.

As the result of the huge concentration difference of emulsions on the two sides of the oil film, the system is in non-equilibrium. The chemical diffusion increases the entropy of a system, which means the emulsion micelles will tend to diffuse through the oil film to bring the system back to equilibrium. In recent studies, oil swelling, mobilization and wettability alteration are considered as the three main mechanisms of emulsification during low salinity water injection [13]. Most direct observations of have been reported for experiments with this phenomenon at very complex environments. Additionally, the emulsion is hard to quantify. Our study will try to obtain this emulsion phenomenon under ideal conditions, and then extend it to reservoir conditions.

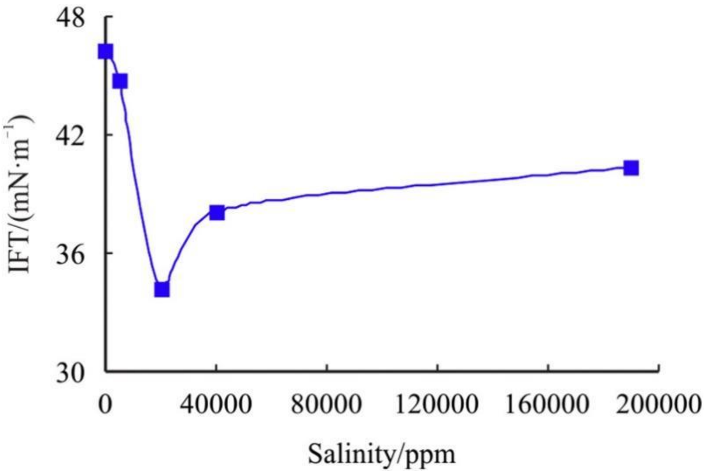

Fig. 25 The IFT of the synthetic oil/water with different salinities [59]

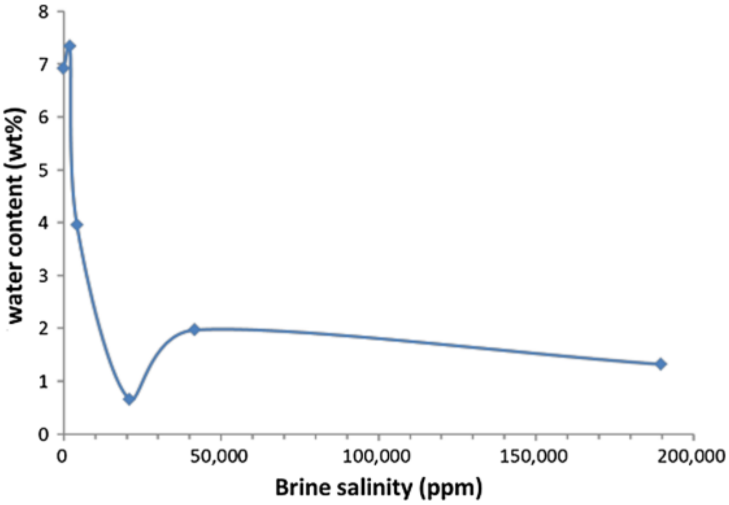

Fig. 26: Water content-Brine salinity relation diagram [16]

Even though the processes of emulsification and osmosis are not clear yet, they are proposed with a consideration of oil as a semi-membrane. Now the questions are, what kind of hydrocarbon can be treated as a membrane; whether the two processes give their contributions on oil mobilization individually; and can we quantify the contributions?

3. Theoretical explanation

3.1. Liquid membrane

Liquid membrane systems involve a barrier liquid layer which is immiscible with both source phase and the receiving phase. If one component of the source phase moves through the membrane faster than another mixture component, this liquid barrier layer can be defined as liquid membrane (LM) [60].

Liquid membrane system is widely used in water treatment, biology, and pharmacy. Three groups of liquid membranes are defined: bulk liquid membrane (BLM), supported liquid membrane (SLM) and emulsion liquid membrane (ELM), as Fig. 27 shown. In our case, two of them are considered as the type of transport system in LSW flooding, the BLM and ELM. The thickness of liquid membrane varied widely, for example the thickness of lipid bilayer in cells can be several nanometers, while some liquid membrane in water treatment can be hundreds of micrometers. This variation in thickness leads to different diffusion methods. Factors that may affect the effectiveness of membrane transportation includes carriers' type, ions properties, temperature, etc., which are still hot topics to study. At this background, a schematic graph can be drawn to illustrate the interaction between oil and water under a salinity gradient for both osmosis and spontaneous emulsification as Fig. 28 shown.

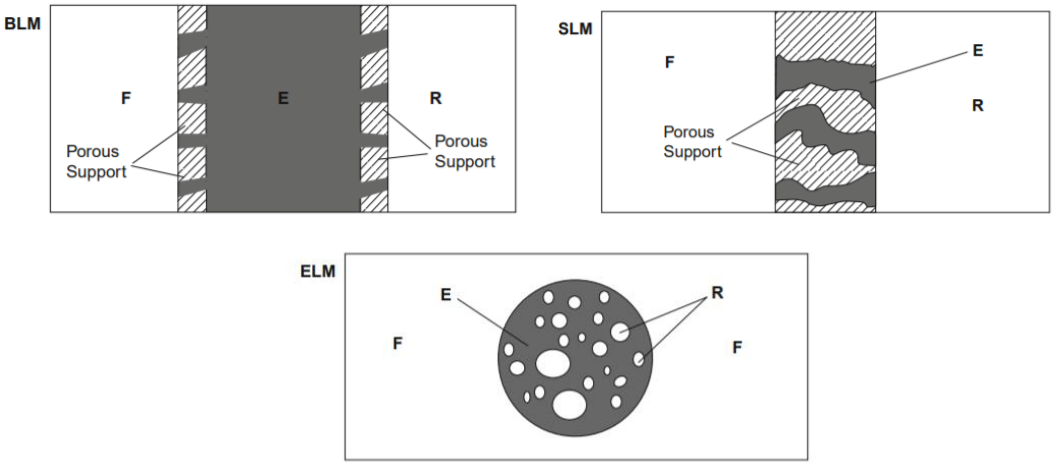

Fig. 27: Three configurations of liquid membrane systems: bulk (BLM), supported (immobilized) (SLM or ILM), and emulsion (ELM). F is the source or feed phase, E is the liquid membrane, and R is the receiving phase. [60]

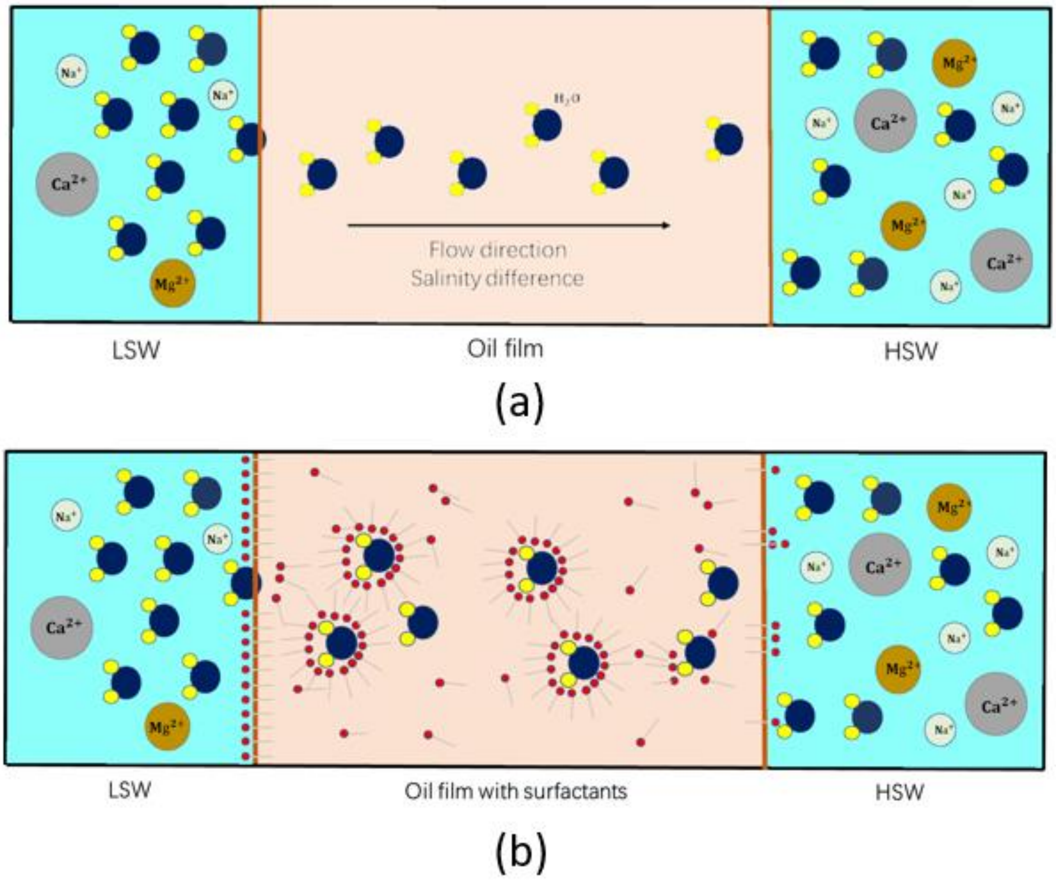
Na⁺
Ca²⁺
Mg²⁺
H₂O
Flow direction
Salinity difference
LSW
Oil film
HSW
(a)
LSW
Oil film with surfactants
HSW
(b)

Fig. 28: The schematic diagram of interaction between oil and water. (a) pure oil under a salinity gradient. (b) surfactants added oil under a salinity gradient.

3.2. Diffusion theory

In terms of thinking about Brownian movement of colloidal particles, Einstein [61] derived a theoretical equation of Fick's law diffusion for small particles with a low Reynold number situation. This relationship is widely used in suspended particle dynamics. In previous studies, Salem [10], Lifei [16], and Pollen [20] used this equation to simplify the water diffusion with microfluidic experiment and one-dimensional capillaries experiment. In dead-end pore system with oil-wet surface, only the water diffusing through the oil phase will be considered with oil wet surface. By Fick's second law, the molecule diffusion can be described by:

$$\frac{\partial c}{\partial t} = D\frac{\partial^2 c}{\partial x^2}$$

where c is the concentration of water in oil, t is time, and x is the distance between two interfaces. D is the diffusion coefficient, which is highly affected by the diffused particles. Fick's second law is used to describe how diffused solute changed with time. The diffusion coefficient, can be estimated it by the Stokes-Einstein equation:

$$D = \frac{k_B T}{6\pi\eta r}$$

where k_B is Boltzmann constant, T is temperature, η is dynamic viscosity of fluid, r is the radius of diffuse particles. As we mentioned above, this relationship is only valid for the spherical particles in a limited Reynolds number environment. For water molecules and reverse micelles in oil phase, a simplification is to approximate these as spherical particles [62].

The water molecules diameter is 3 Å. Emulsion reverse micelles, made of about 100 surfactant molecules, the size may range from 10 to 1000 Å [63]. The diffusion time scale is $x^2/2D$, where x is the thickness of the oil film. For typical situations, the dynamic viscosity of n-heptane is $3.76 \times 10^{-4}\ Pa \cdot s$ and for n-dodecane is $1.36 \times 10^{-3}\ Pa \cdot s$. The detailed information of the material will be introduced in section 4.1. By data supported by Salem [10], we also know that ions' diffusion rate is two orders lower than water. Basically, we can ignore the diffusion of ions in our ideal model.

4. Materials and methods

4.1. Experimental design

In this study, multiple experimental methods were employed to study the effect of osmosis and spontaneous emulsification during LSW water flooding: microfluidic, dynamic light scattering (DLS) and pendant drop observation. The microfluidic experiments are used to give a direct visualization of liquid interface movement and interfacial reaction. The DLS can supply the size of the micelles of water in oil emulsion. And the pendant drop observation can give us a better understanding of spontaneous emulsion accumulation on water surface. To have a better visual effect, we used synthetic oil rather than crude oil in our experiments. Previous studying indicated that heptane has the best performance as a semi-membrane among the tested hydrocarbon substances [35]. However, the study of higher alkanes (C7+) as semi-membrane is still absent. Based on these considerations, we select the n-heptane and n-dodecane as our target hydrocarbon. For emulsifier, we used SPAN 80 (Sorbitane monooleate, HLB=4.3). Brine samples with salinity of 0, 1700, 17000, 50000 and 170000 ppm were prepared using multiple salts as shown in Table 2. High-salinity brine was synthetically made by mixing deionized water and different amounts of pure salts to gain a 20% w/v solution. The salts used in this study are $NaCl$, KCl, $MgCl_2$, and Na_2SO_4. To avoid the gas generation, we did not add $NaHCO_3$. Also, to avoid ion concentration difference between oil and brine, both dodecane and heptane are equilibrated by placing them with HSW for two days. Refined oil was colored with Oil Red O. Brines were colored with Methyl Blue. Because very little of the colorant was used to dye our fluids, the effect on the LSW salinity can be ignored. All the salts and coloirants are supplied by Sigma Aldrich.

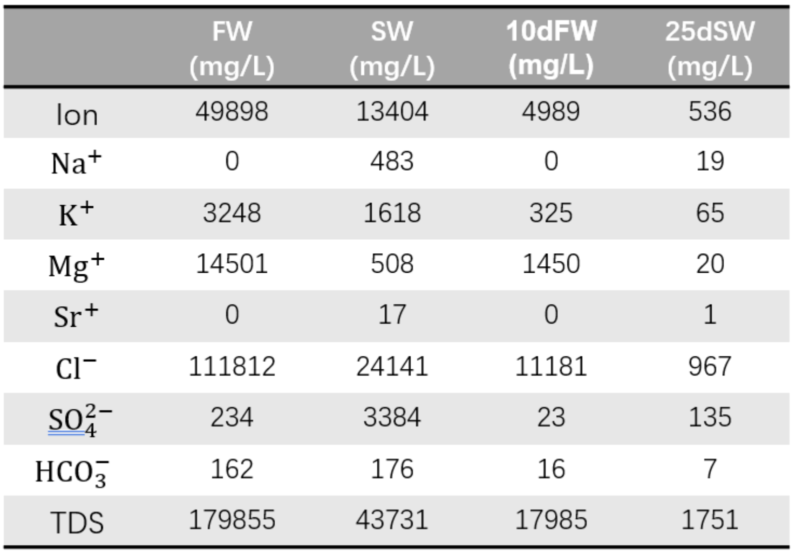

	FW (mg/L)	SW (mg/L)	10dFW (mg/L)	25dSW (mg/L)
Ion	49898	13404	4989	536
Na^+	0	483	0	19
K^+	3248	1618	325	65
Mg^+	14501	508	1450	20
Sr^+	0	17	0	1
Cl^-	111812	24141	11181	967
SO_4^{2-}	234	3384	23	135
HCO_3^-	162	176	16	7
TDS	179855	43731	17985	1751

Table 2: The brines are prepared by mixing deionized water and different amounts of pure salts. The FW composition is taken from Middle Eastern carbonate field. [64]

4.2. Microfluidic experiment set-up

As we mentioned in section 2.3, microfluidic experiments are widely used to observe the osmosis and spontaneous emulsification during low salinity water flooding. Microfluidic experiments are designed to visualize pore-scale fluid movement. The main difference between the behavior of fluids at the pore level versus larger scales is that gravity and inertia no longer play a dominant role. Surface tension, energy dissipation, and fluid resistance begin to dominate fluid behavior. The small size micromodels can imitate real reservoir rock systems in a convenient setup to some extent.

The micromodel used is provided by Micronit. The chip is designed with randomly placing rock shape structures to resemble the actual shape of real rock, as shown in Fig 28. The total permeability of the chips is 2.5 Darcy, and the porosity is 57%. More information of the chips we used are listed in Table 2. The material of the chip is borosilicate glass, which is similar to quartz.

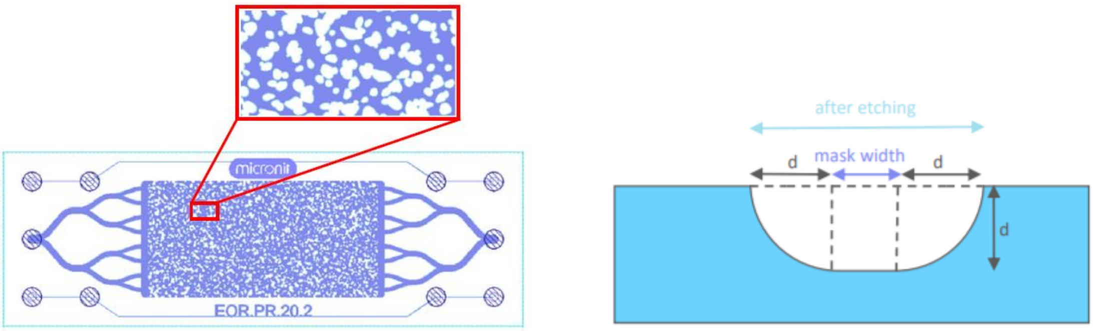

Fig. 29: EOR physical rock network microfluidic chip supplied by Micronit

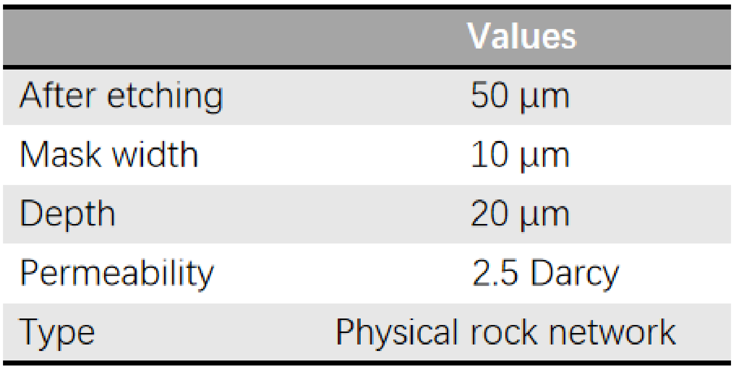

	Values
After etching	50 µm
Mask width	10 µm
Depth	20 µm
Permeability	2.5 Darcy
Type	Physical rock network

Table 2: Channel information for micro chips

The observation platform is an OLYMPUS SZX-7 microscope with a UC90 camera, connected with a computer screen. The microfluidic system we used is shown as Fig. 30. The system is also sketched below as Fig. 29 showed. The syringe pump connected to the left side of the micro-chip, which is aimed to inject the fluid with a constant rate. The vacuum pump is connected with a valve, so that we can switch it to the waste collector after we finish the suction.

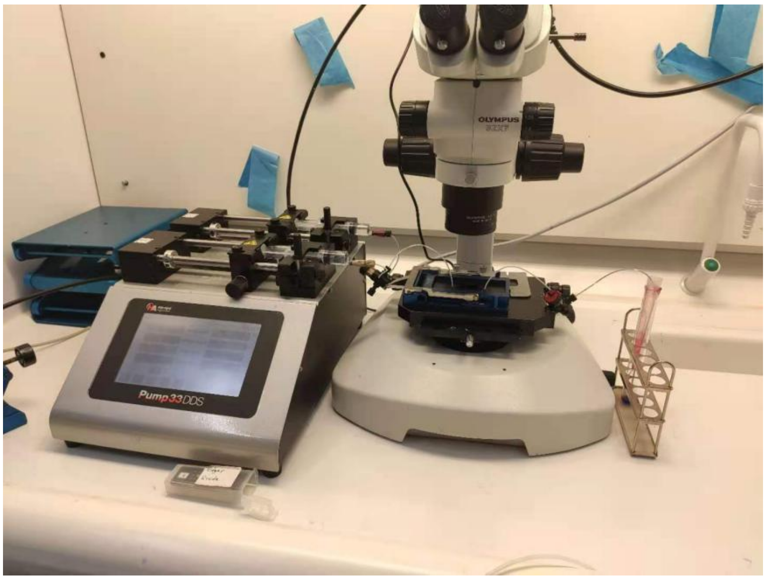

Fig. 30: Photo of microfluidic system

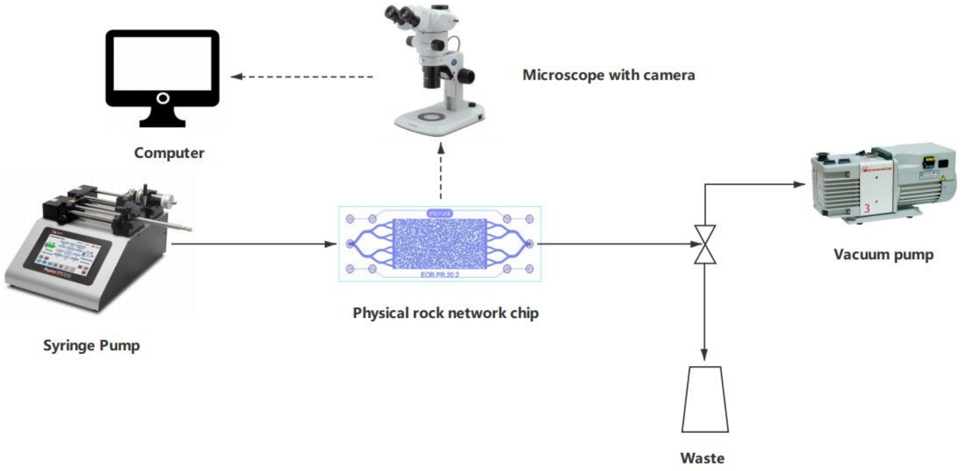

Fig. 31: A schematic picture of the microfluidic system

To obtain oil-wet chips we used SilicaSafa with heptane to change the wettability and methanol to wash out the wetting agent. The SilcaSafa/heptane fluid should keep injecting for 10 minutes to ensure the micro-chips altering to oil wet. After 24 hours drying, we vacuumed all the air in our system by a vacuum pump, and then injected high salinity brines, as Fig. 32 (a) shown. To study the mechanism of emulsification, microchips were filled with 170000 ppm water as connate water at the beginning. Then, we injected oil with 100 µl/min to seal the high salinity water as a trapped water, this replicate the primary drainage in the reservoir as Fig. 32 (b) shown. A high oil rate is necessary in such oil wet system as the trapped water is easily to be washed out with a relatively low oil rate. After the system is in equilibrium, we inject low salinity water with a very low rate of around 5 µm/mins until the front reach to the outlet. At last, we close the outlet and inlet, creating an isolated environment for the system. We then waited 30 mins for the system to the equilibrium. Fig. 32 (c) illustrates the chip after the procedure.

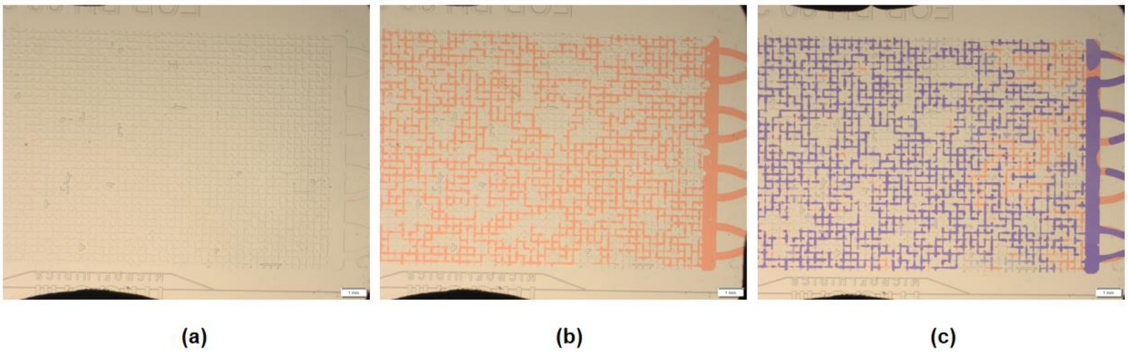
(a) (b) (c)

Fig. 32: The procedure of the microfluidic experiments. (a) Vacuum the chip and inject the HSW (b) Inject oil (red) (c) Inject LSW and displace oil

The observation area will look like Fig.31. Here we take the experiments with heptane as example. The clear white area is connate water, which is surrounded by grains and oil. The red part is the oil phase (heptane or dodecane in our cases), and the blue is the LSW. Because the surface in the microchips was altered to oil wet, the HSW zone is fully surrounded by the oil phase at this situation. If the volume of HSW expands, the only pathway for water is by diffusing into the oil phase and transporting through the oil film.

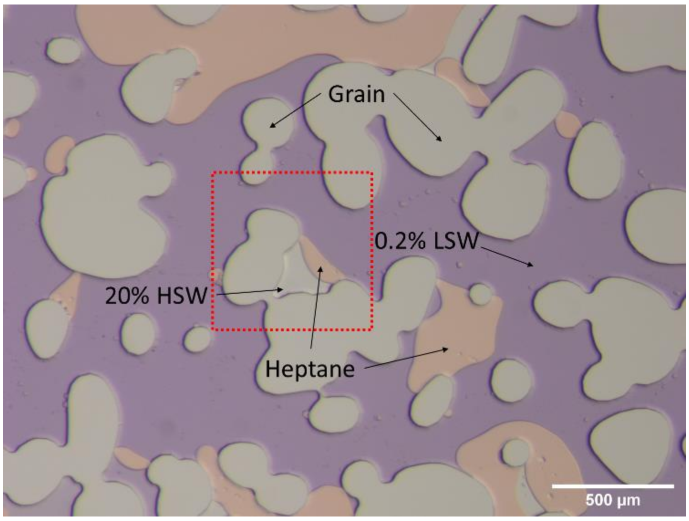

Fig. 33: The microfluidic experiments view under the microscope`

Dynamic Light Scattering (DLS) was used to measure the micelles size of emulsions. We used Zetasizer 90, which was provided by Malvern Panalytical (see Fig. 34). Dynamic light scattering (DLS) is a technique that determining the size distribution profile of small particles in suspension or polymers in solution [38]. A monochromatic light source, usually a laser, shot through a polarizer and into the sample. The scattered light then goes through a second polarizer, where it is collected by a photomultiplier with the resulting image projected onto a screen. For different size of the particles, the Brownian motion of these particles or molecules causes the intensity of the light they scatter to fluctuate rapidly. Analysis of these short-term intensity fluctuations yields the speed of the Brownian motion, which is used to calculate the particle size with the Stokes-Einstein relationship. The sample chamber for Zetasizer is shown below (Fig. 34). To study the emulsion properties generated by spontaneous emulsification, we set up a one interface model with different salinity brines covered by oil at the top. The emulsion generation zone height is the same as laser height to detect the emulsion size change vis time. The schematic picture of the spontaneous emulsification in the test chamber is illustrated as Fig.35 shows. To compare the effects to the observation in the microfluidic experiments, we used the same brines as they were used in the microfluidic experiments i.e., 0 ppm, 1700 ppm, 17000 ppm, 50000 ppm and 200000 ppm.

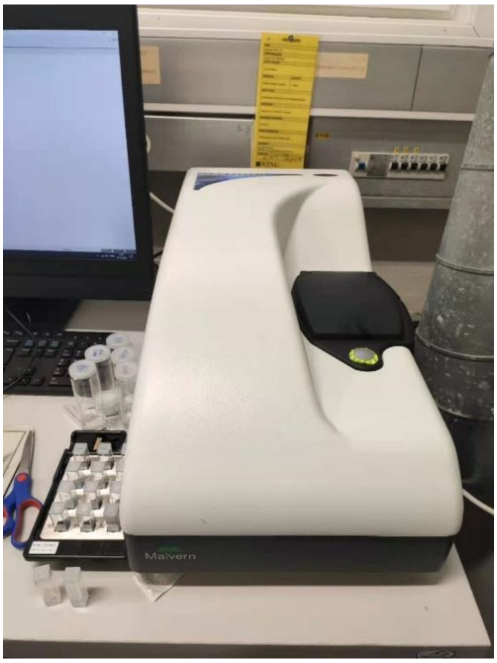

Fig. 34: Dynamic light scattering device is Zetasizer ZS90 from Malvern Panalytical.

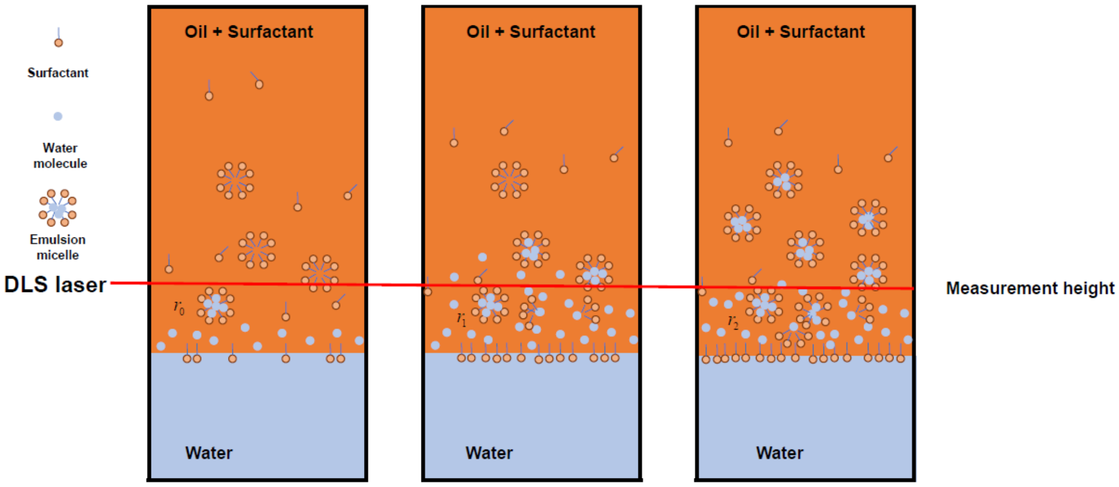
Surfactant
Water molecule
Emulsion micelle
DLS laser
Oil + Surfactant
Oil + Surfactant
Oil + Surfactant
r_0
r_1
r_2
Measurement height
Water
Water
Water

Fig. 35: A schematic illustration of the spontaneous emulsification in the DLS chamber

4.3. Pendant drop experiment set-up

Pendant drop tensionmetry offers a solution to determine surface and interfacial tension and observe the droplet behavior in many colloidal systems. An experimental investigation of spontaneous emulsification is proposed with a water drop pendant in a refined oil environment with a surfactant added. The experimental apparatus consists of a camera, a dispensing system, and the light source. The drop shape analyzer we used is supplied by KRUSS DSA100E.

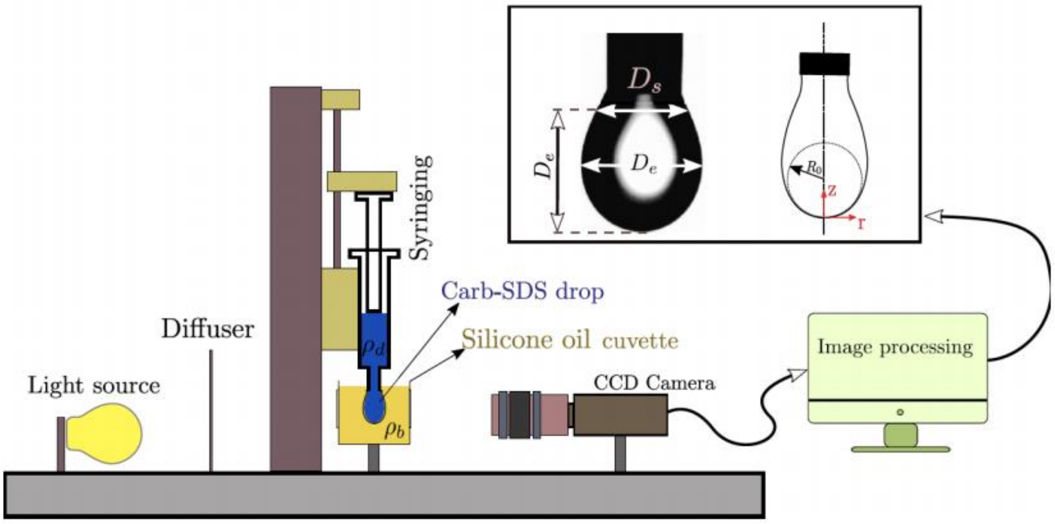
D_s
D_e
D_e
R_0
z
r
Syringing
Carb-SDS drop
Silicone oil cuvette
Diffuser
Light source
ρ_d
ρ_b
CCD Camera
Image processing

Fig. 36: Sketch of the pendant drop experimental apparatus [65]

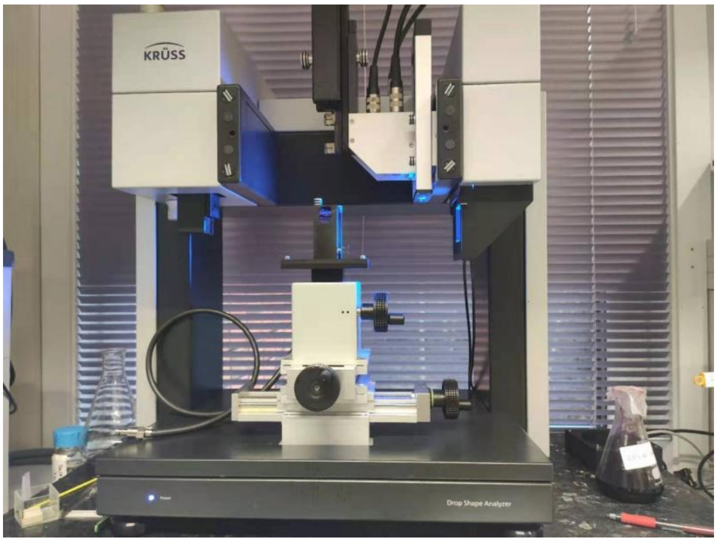
KRÜSS
Drop Shape Analyzer

Fig. 37: Drop shape analyzer DSA100E by KRUSS

5. Experimental results

5.1. Microfluidic experiments results

To study the osmosis and emulsification effect in low salinity water flooding, a series of microfluidic experiments were conducted. Table 3 lists the experiments that we set in n-heptane and n-dodecane with or without surfactant. Meanwhile, different salinity brines were also used to study the effect of the concentration of salts. From the literature, we already know that the optimum salinity for low salinity injection is around 2000 ppm brines. So, for comparison, we set the LSW at 1700 ppm as the optimum, while we consider 50000 ppm moderate and 200000 ppm HSW. In following sectionThe oil phase can act as a semi-permeable membrane when a salinity gradient is established [12]. We set up baseline experiments with equal salinity in the connate water and injected brines with both surfactants and no surfactants added to the oil. In total, there were 16 experiments conducted on microfluidic listed in the Table 3. And the measurements of the connate water for all 12 experiments are shown in Fig. 38.

The results will be discussed based on our observation and compared to the literature. Meanwhile, we will also discuss some assumptions and models for oil semi-membrane systems in Chapter 6.

Exp #	Connate water	Brine	Oil	Surfactants	Inf.
Exp 0a	1700 ppm LSW	1700 ppm LSW	n-Heptane	/	Base line
Exp 1a	200000 ppm HSW	1700 ppm LSW	n-Heptane	/	
Exp 2a	200000 ppm HSW	50000 ppm HSW	n-Heptane	/	
Exp 3a	200000 ppm HSW	1700 ppm LSW	n-Heptane	1% SPAN80	
Exp 4a	1700 ppm LSW	1700 ppm LSW	n-Heptane	1% SPAN80	Base line
Exp 5a	200000 ppm HSW	1700 ppm LSW	n-Heptane	2% SPAN80	
Exp 6a	200000 ppm HSW	50000 ppm HSW	n-Heptane	1% SPAN80	
Exp 7a	200000 ppm HSW	50000 ppm HSW	n-Heptane	2% SPAN80	
Exp 0b	1700 ppm LSW	1700 ppm LSW	n-Dodecane	/	Base line
Exp 1b	200000 ppm HSW	1700 ppm LSW	n-Dodecane	/	
Exp 2b	200000 ppm HSW	50000 ppm HSW	n-Dodecane	/	
Exp 3b	200000 ppm HSW	1700 ppm LSW	n-Dodecane	1% SPAN80	
Exp 4b	1700 ppm LSW	1700 ppm LSW	n-Dodecane	1% SPAN80	Base line
Exp 5b	200000 ppm HSW	1700 ppm LSW	n-Dodecane	2% SPAN80	
Exp 6b	200000 ppm HSW	50000 ppm HSW	n-Dodecane	1% SPAN80	
Exp 7b	200000 ppm HSW	50000 ppm HSW	n-Dodecane	2% SPAN80	

Table 3: Microfluidic experiments with SPAN80 to study spontaneous emulsification effect and without SPAN80 to study the osmosis effect (a: experiments with n-heptane; b: experiments with n-dodecane)

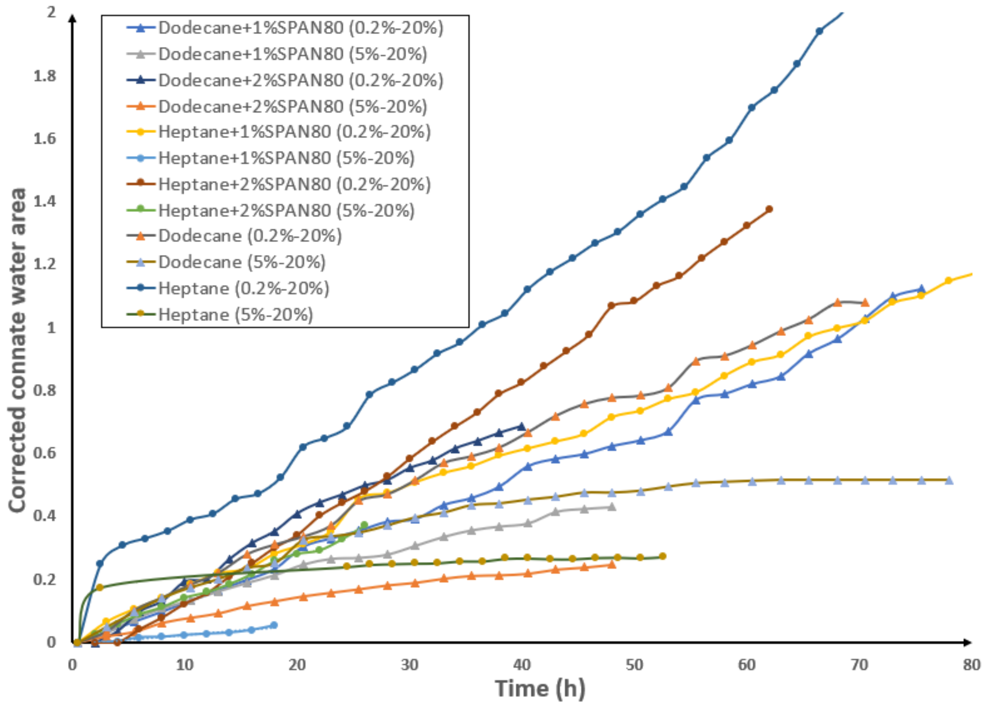

Fig. 38: The corrected connate water area changes vis time for all the microfluidic experiments

5.1.1. Brine injection without surfactant added

Some studies [13] [10] [45] proposed that the oil phase can act as a semi-permeable membrane that allows the osmotic water transport in oil. We observed that the HSW region isolated by pure alkane expanded after several days. For the experiment without surfactant added, the osmosis causing water transportation during the low salinity water flooding is studied. In this study, the n-heptane and n-dodecane are selected as the oil phase. Experiment 0a and 0b are conducted with equal salinity brines as connate water and injected water as Fig. 38 and Fig. 41 shown. Experiments 1, 2 and 3 are conducted without surfactant. To be simplified, we use percentage to present the salinity of brines and 1700 ppm is rounded to 0.2%.

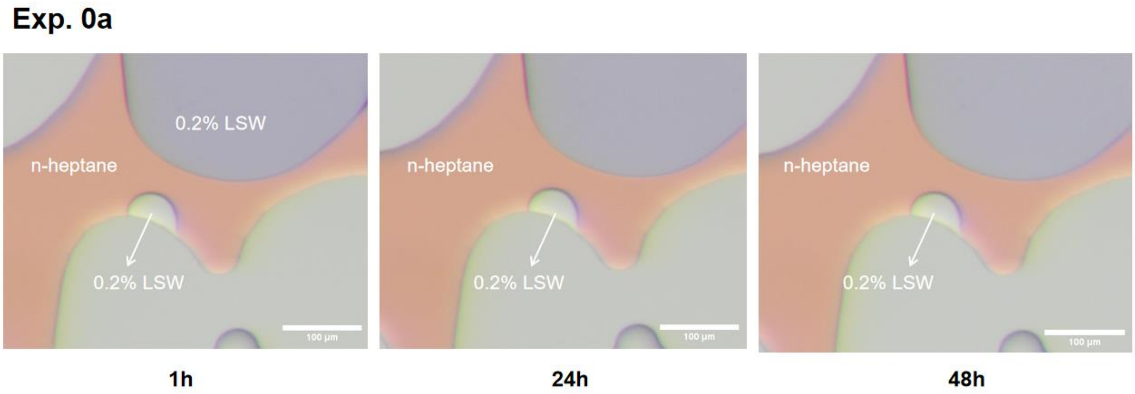

Fig. 39: No area changes of connate water with equal salinity brines.
Top is heptane/0.2% LSW and bottom is heptane/5% LSW.

From Fig. 39 we can see that all the connate water in Exp.1a (0.2% LSW) has an obvious swelling after 48 hours. However, comparing with the change in 0.2% LSW, the connate water in the Exp. 2a with 5% LSW injection shows less size change. The experiments with dodecane also shows a similar phenomenon. The connate water swelling for dodecane with 5% LSW is much faster compared with the heptane. Fig. 40 shows the image that we measure for the dodecane.

The connate water expands after the LSW was injected into the system. We evaluate the size change for both heptane and dodecane. To minimize the influence by the shape and size difference of connate water for different experiments, we used the corrected water flux that derived by the Fick’s law to help us compare the water flux (the derivation and the method will be introduced at the end of this section, p47). The Fig. 41 shows the curve of the corrected water flux. It should be noted that the distance between the HSW and the LSW is varied as the HSW expands. So, the curve of the water flux can only show the trend of the rate of the water.

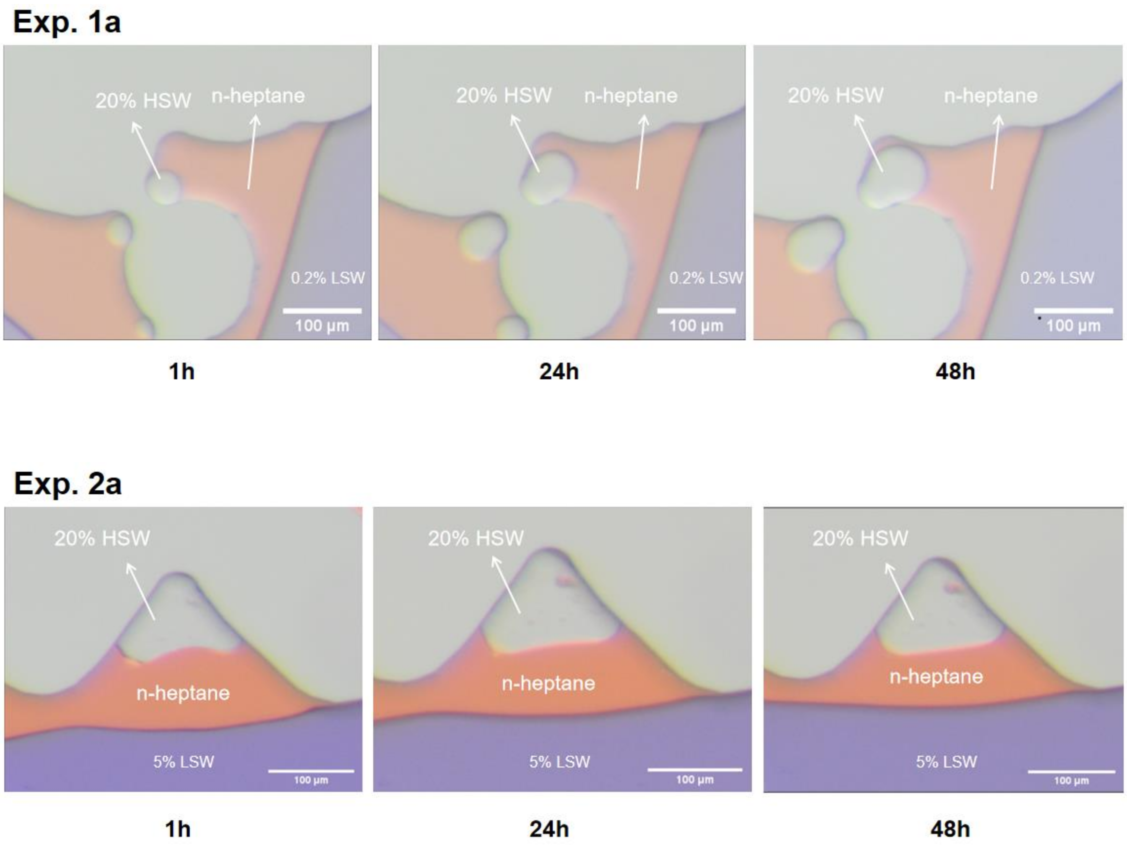

Fig. 40: Images of the isolated HSW area after 1-hour, 24-hour and 48-hour. Top is heptane/0.2% LSW and bottom is heptane/5% LSW.

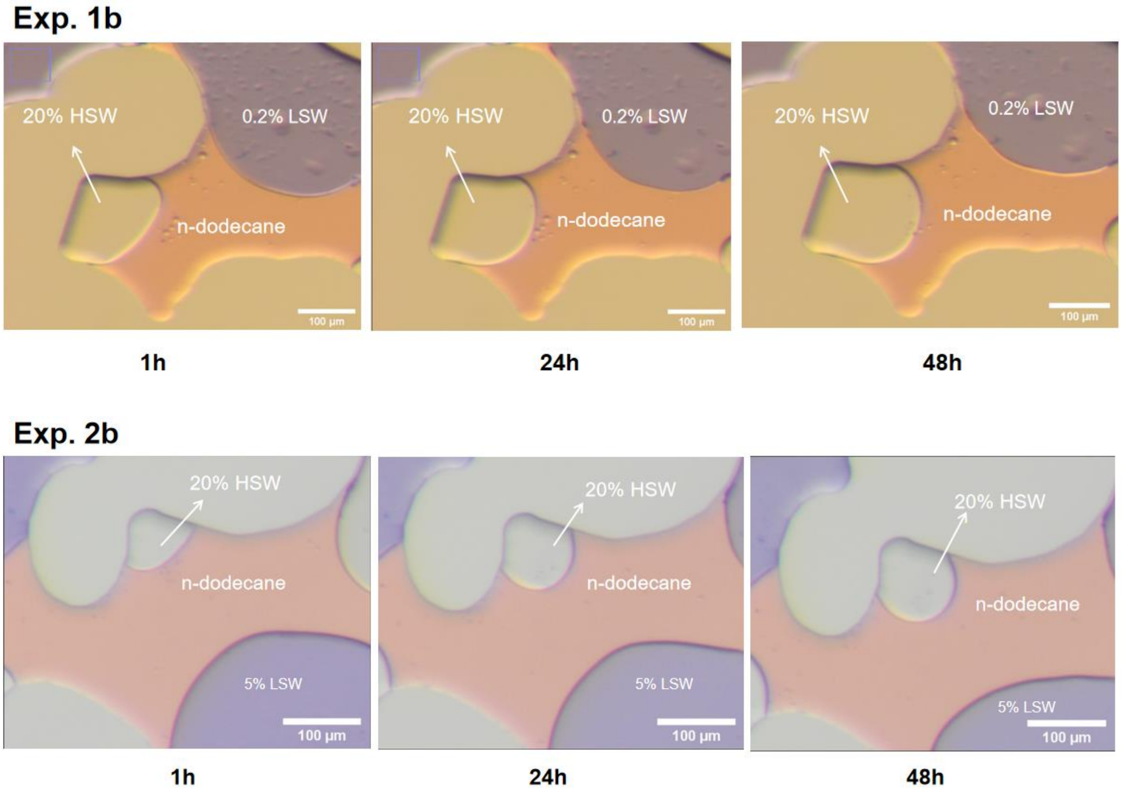
Exp. 1b
20% HSW
0.2% LSW
n-dodecane
100 µm
1h
24h
48h
Exp. 2b
20% HSW
n-dodecane
5% LSW
100 µm
1h
24h
48h

Fig. 41: Images of the isolated HSW area after 1-hour, 24-hour and 48-hour. Top is dodecane/0.2% LSW and bottom is dodecane/5% LSW.

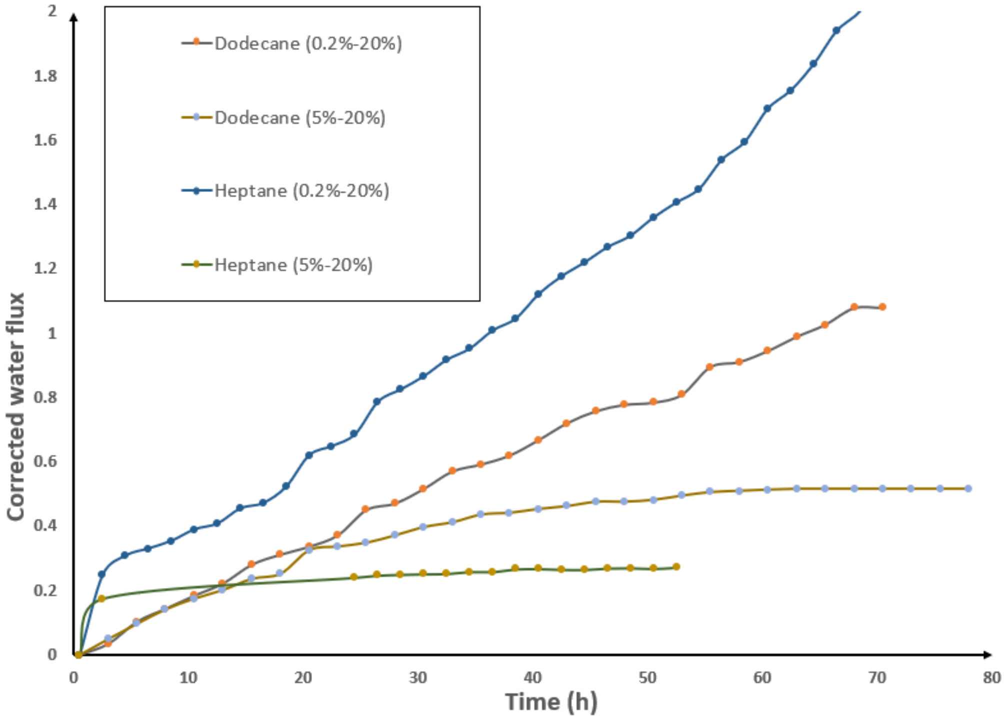

Fig. 42: Curves of the variation in HSW area versus observation time for the oil phase without surfactants in the oil phase

5.1.2. Brine injection with surfactant added

The other groups of microfluidic experiments were performed with surfactant (SPAN-80) added into the oil phase (n-Heptane and n-Dodecane). To investigate the effect on water transportation by adding surfactants to create spontaneous emulsion at the water/oil interface, we performed 8 experiments with 1%-2% w/w SPAN 80 added. Meanwhile, two baseline experiments with equal salinity were set as references. Fig. 43 shows the graphs of one of the baseline experiments. Comparing with the reference group, with the equal salinity of 0.2%, the expands of connate water is negligible. Fig. 44 illustrate one example with 1% SPAN 80 added to n-dodecane and the salinity of brines are 0.2% and 20% as LSW and HSW. The other experiments had the similar phenomena of HSW expands.

It is obvious that the HSW area increase dramatically. At the beginning and up to 20 hours the area of HSW increase moderately. As the distance between the HSW and the LSW decrease, the HSW area grows faster. After 70 hours, the oil film become a very thin oil layer and the HSW area increases much faster than before. This indicates the relationship between the water transportation rate and the thickness of the oil layer. During the first 60 hours, the area increases about 49.8%. In contrast, the area increase from 60 to 80 hours is around 84%.

To compare the effect of different salinity, Fig. 41 shows an experiment with 5% LSW. The area increases about 24.1% during the first 24 hours, and 36.5% between 24 and 48 hours. As the width of oil phase separating the LSW and HSW is similar but the affecting HSW/oil interface for the 5% LSW is larger than 0.2% LSW shown in Fig. 43, the HSW area increase is similar for the first 24 hours. After 24 hours, the area increase became slower for the current 5% experiment. This is due to the increased distance between HSW and LSW.

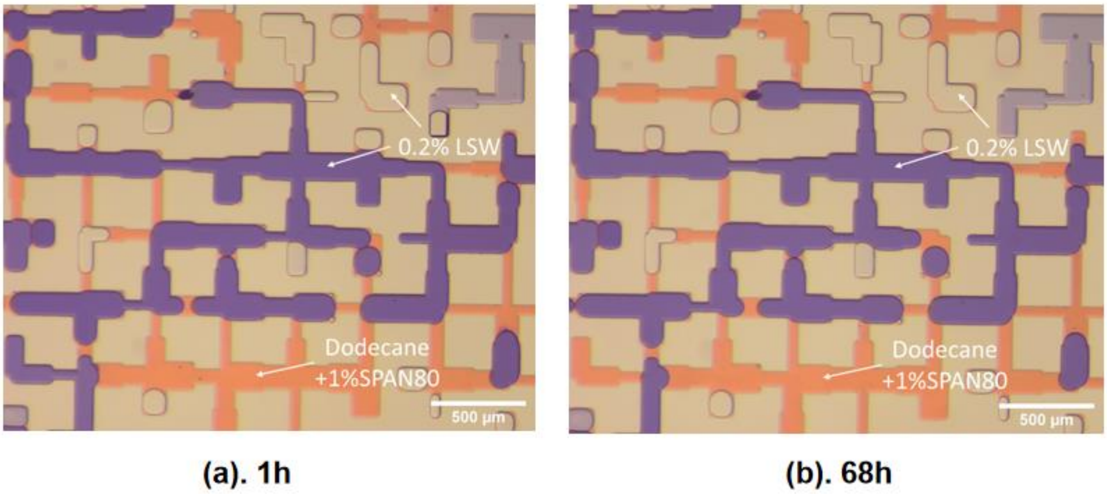

Fig. 43: Images of the reference experiments LSW/Oil/LSW system for surfactants adding. The area increase for connate water is negligible. (Exp. 4b)

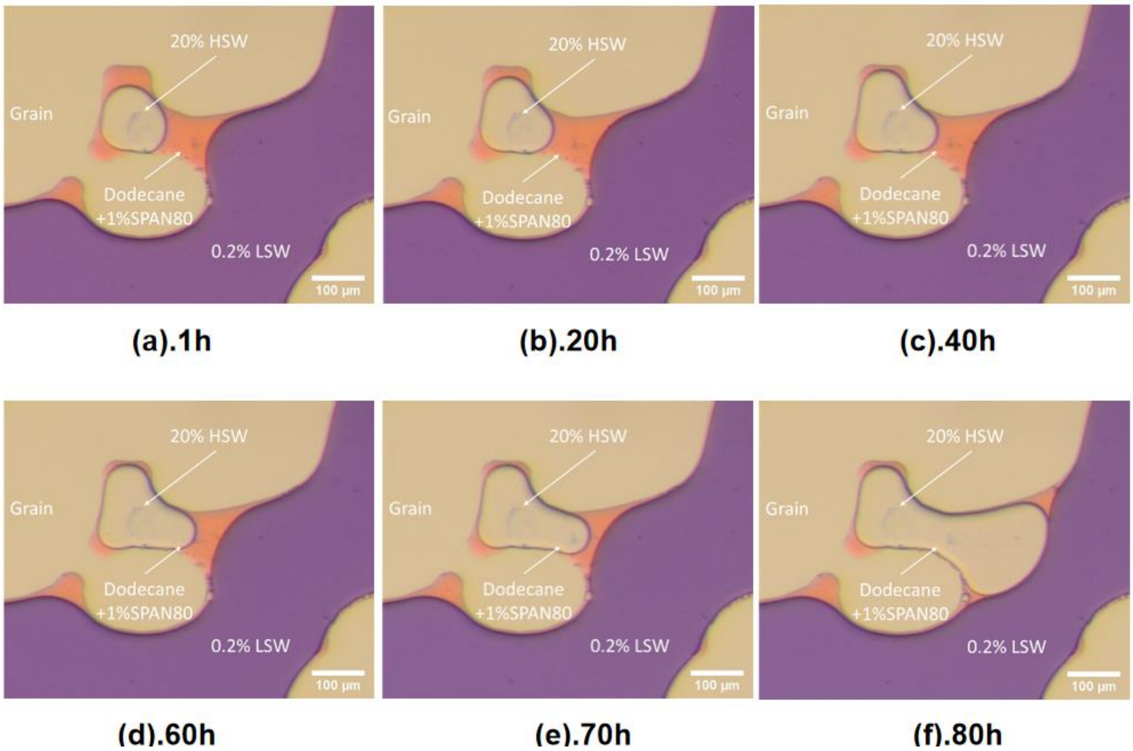

Fig. 44: Images of the isolated LSW/Oil/HSW system with surfactants added to the oil imaged from 0 to 80 hours. (Exp. 3b)

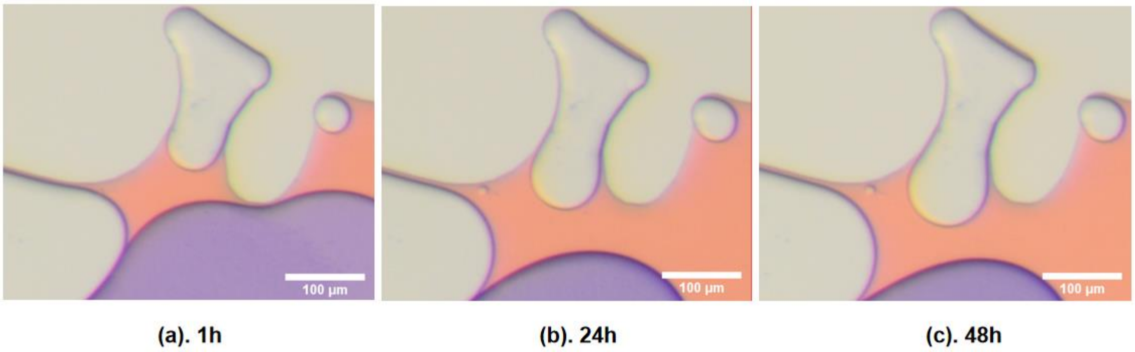

Fig. 45: Images at 1h, 24h and 48h of the 1% SPAN 80 dodecane with 5% brine as LSW

We also investigated the effect of changing the amount of surfactant in the oil phase. In Exp. 6 and Exp. 8, the surfactant amount is doubled to 2% w/w SPAN 80 added to the oil phase. In the experiments with 2% SPAN 80, a clear supersaturation zone was observed in the case with 0.2% LSW. Fig. 45 (a) shows the generation of the supersaturation zone. The brown material is the mixture of connate water (20% HSW) and the dodecane with 2% SPAN 80, generated by the primary oil displacement. The mixture is not stable due to the high salinity of the aqueous phase. The mixture finally separated with two phases. From Fig. 45 we can observe emulsions accumulated at the left of the throat, a super- saturation zone. Black points and large water bubbles were observed in this region. The super- saturation zone seemed stable, as there were no observed differences with time. The Fig. 46 shows the emulsion accumulation at the LSW/Oil interface. The system is the same as Fig. 45, with 2% SPAN 80 in the oil and 0.2% LSW and 20% HSW. Only the experiments with 2% SPAN 80 can observe this phenomenon. The mechanisms of the visible emulsion accumulation or visible supersaturation zone is still hard to define. Possible influence factors are surfactants concentration, pore structure, and the initial environment energy level (injection rate, temperature, and pressure).

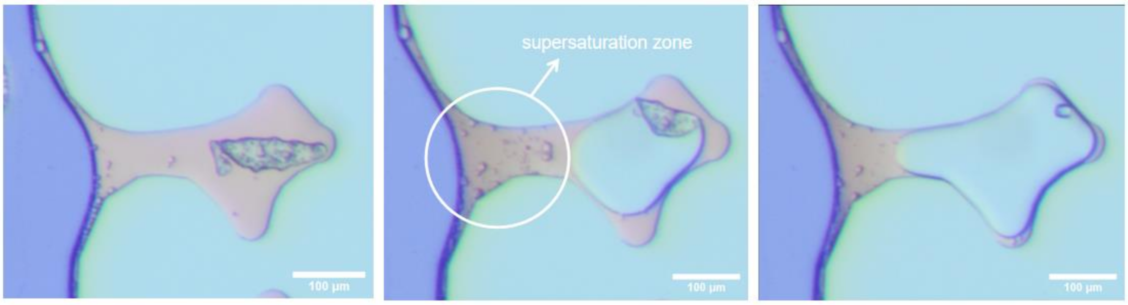

(a). 1h (b). 24h (c). 34h

Fig. 46: Images at 1h, 24h and 34h of the 2% SPAN 80 dodecane with 0.2% brine as LSW.

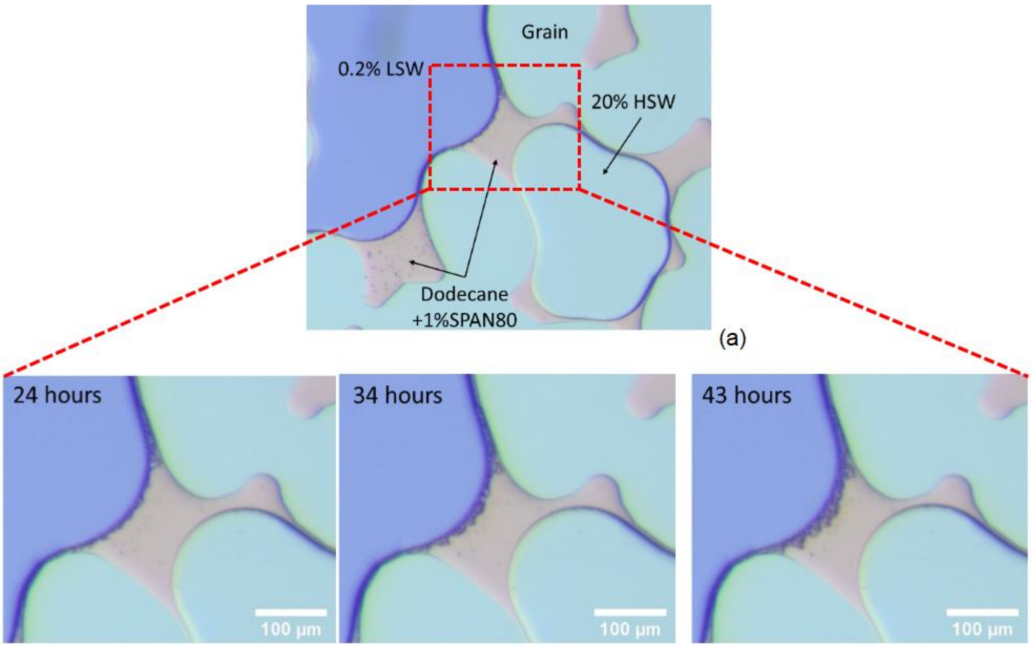

(b) 24 hours (c) 34 hours (d) 43 hours

Fig. 47: Spontaneous emulsion accumulation was observed after the LSW flooding. (a) picture of the selected LSW/Oil/HSW system; zoomed images giving a close view of the brine-oil interfaces showing the change in emulsion behavior after 24 hours (b), 34 hours (c), and 43 hours (d).

To compare the water transportation rate for different oil and salinity gradient, we used corrected water flux to represent. The corrected water flux is derived by Fick’s law, which is given by:

$$\frac{\partial c}{\partial t} = D\frac{\partial^2 c}{\partial x^2}$$

Considering the flux in transit time, the equation can be:

$$\boldsymbol{q}' = -\frac{M}{\rho} \cdot D \cdot \frac{\partial c}{\partial x}$$

q' is the flux in transit time, *D* is the diffusion coefficient, *c* is the water concentration, and the *x* is the distance between the HSW and the LSW. Then, change the flux to the area change with time, we will have:

$$\frac{dA}{dt} = \frac{\boldsymbol{q}' \cdot S}{h} = -\frac{M}{\rho} \cdot D \cdot \frac{dc}{dx} \cdot \frac{S}{h}$$
$$\frac{dA}{dt} = \frac{M}{\rho} \cdot D \cdot \frac{dc}{dx} \cdot L$$

The *S* is the contacting area between the HSW and the oil. The contacting area is the area that have the water transportation, not include the HSW area contacting with the grain. The area divided by height of the micro-chip is the contacting length of the HSW zone. The length is varied during the HSW expands so that we only consider the initial length. By organizing the equation, we will have:

$$\frac{\Delta A \cdot \Delta x}{L} = \frac{M}{\rho} \cdot D \cdot \Delta c \cdot \Delta t$$

For different connate water, the shape is also varied. The area of the connate water surrendered by the grain have no effect on the water transportation. If this area was large, the relative area only has slight change during the HSW zone expands. To decrease the influence by the shape of the HSW area, all the observation objects are calibrated by setting a reference circle, which is created basing on their arc at initial situation. The outline of the reference circle should fit for HSW reaction interface as much as possible. Fig.47 shows one example of our calibration. Meanwhile, the effect of the length of the arc will be covered by the area of the reference circle. At last, the equation will be:

$$\Delta A_{relative} \cdot \Delta x = \frac{M}{\rho} \cdot D \cdot \Delta c$$

and

$$A_{relative} = \frac{(A_n - A_1)}{A_{reference}}$$

Where A_n is the HSW area at different time, and the A_1 is the HSW area at the initial time.

As all our observation measurements calibrated by the circle, the rate of the water transportation can be defined by the area change of HSW zone multiply the distance between the HSW and the

LSW, which is the slope of the corrected area change curves. In the calculation of the corrected water rate, we also consider the Δx as the initial distance between the HSW and LSW to simply our calculation. This calibration is not totally precise. But it can also eliminate part of the error that caused by the shape of observation zone. Fig. 48 shows the HSW area change for the experiments with surfactants added. In Chapter 6, we will have a detailed discussion of the results.

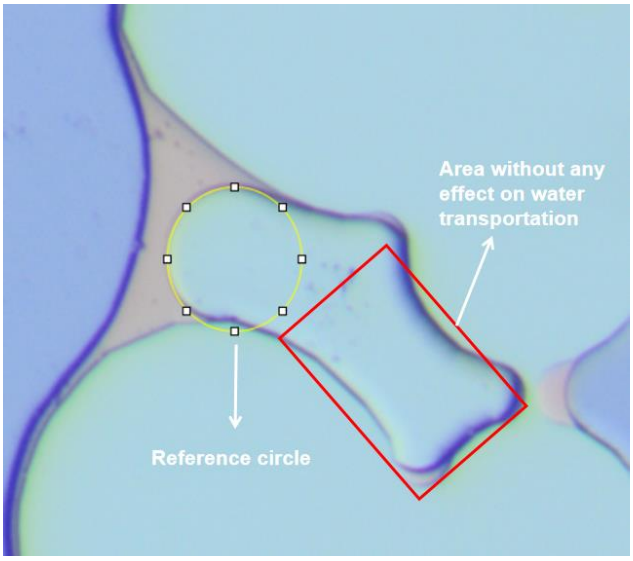

Fig. 48: The reference circle needs to fit the reaction interface of HSW as much as it possible.

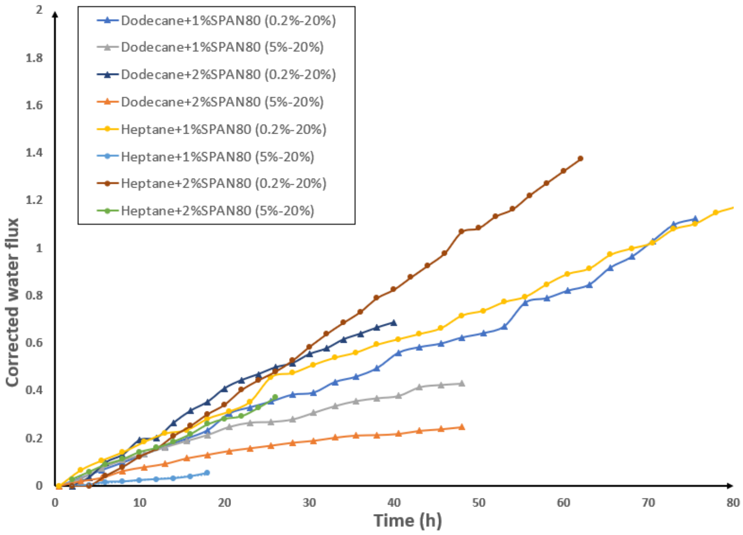

Fig. 49: Curves of the variation in HSW area versus observation time for the oil phase with surfactants adding

5.2. Light scattering experiments results

In our light scattering experiments, we measured the spontaneous emulsion droplet size with the same fluids as the one used in the microfluidic experiments. The size change of emulsion droplets and the emulsion accumulation may affect water transportation rate [10]. Fig. 50 shows images of the spontaneous emulsification process for 1700 ppm brines with 1% SPAN 80 / dodecane for 27 hours. No obvious emulsion that can be visually observed. After two hours some white turbidity appeared on the oil water interface, where concentration of micelles is gradually increasing. At around 5 hours, we can see that white smokey dispersion appeared at the upper oil water interface. These white smokey dispersion are shaped by large emulsion droplets created by many small micelles due to the Ostwald ripening [66]. After around 7 hours the large emulsion droplets precipitated on the interface again due to gravity effects. However, the size of these emulsion droplets can be different because of hydrated ions concentration in the oil phase. We will discuss this in chapter 6.

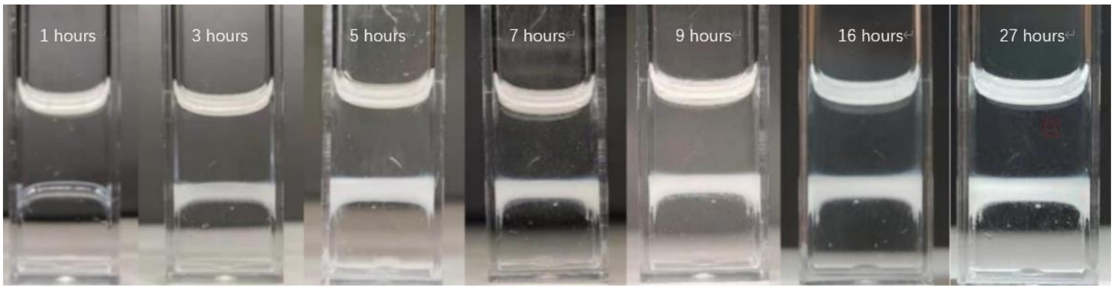

Fig. 50: Dodecane with 1% SPAN 80 contacting with 1700ppm brines. Emulsions deposits after 3 hours and got thicker subsequently.

Dynamic light scattering experiments gave a detailed description of the spontaneous emulsion size change process. The value also fit the visual observation results well. 16 sets of experiments were used to study the salinity and surfactants effect on the spontaneous emulsion generation. Fig. 51 shows the measurements of the emulsion droplets size vis time for dodecane and heptane with two typical salinities (low: 0.2% w/w salt, moderate: 5% w/w salt). For dodecane with 1% SPAN 80, the emulsion size distribution has two peaks, one is around 10 nm and the other one is around 1000 nm. In Fig. 51a, we can observe that for 0.2%, the size distribution become steady after 4 hours. The intensity of emulsion at peak 1 (10 nm) goes down during the first 4 hours, while the size of peak 2 vary. For the sample with 5% salts, a similar change is not easy to recognize, and the intensity of peak 1 is relatively high compared with the 0.2%, which indicates a higher composition of small size emulsions in the 5% sample. For heptane with 1% SPAN 80, the emulsion size distribution is not very stable. We can see that the intensity of peak 2 (500 nm) is decreasing with the time, while peak 1 (10 nm) is increasing. There are no small size emulsions in heptane with 5% salts brine at the beginning, as the smallest emulsion size is around 250 nm for the first 3 hours. After 24 hours, it shows a combination with various size of micro-emulsions. However, for heptane with 0.2% salts brine, only the small emulsion survives to the end.

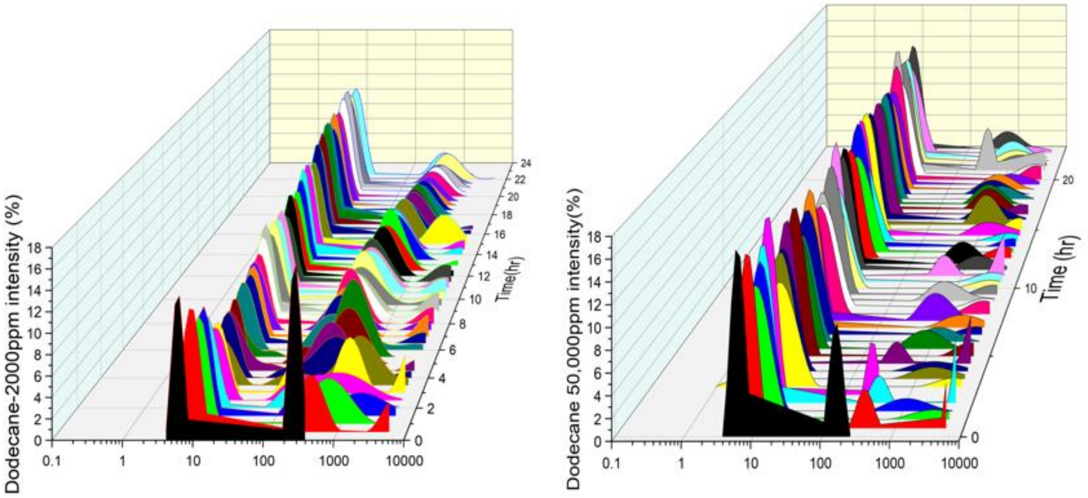

(a). Dodecane 1% SPAN 80 (Left: 0.2% Right: 5%)

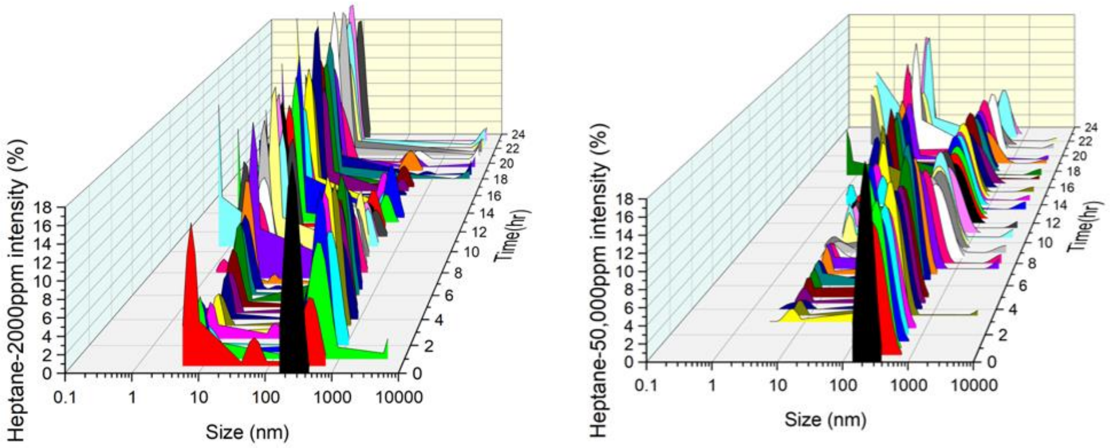

(b). Heptane 1% SPAN 80 (Left: 0.2% Right: 5%)

Fig. 51: The emulsion size distribution vis time for heptane and dodecane with 1% SPAN 80 that contacting with 0.2% and 5% salts brine.

In Fig. 52, we can see that the emulsion size distribution changed as the contacting brine salinity is increasing. For dodecane, the emulsion size with all salinity brines is more stable than heptane. DIW, 5% and 20% cases show a strong similarity between the emulsion size distribution and intensity. However, the intensity or the proportion of larger micro-emulsion for 0.2% is much larger than the other cases at the first 20 hours. This phenomenon that may relate to performance of the water transportation as we will discuss in Chapter 6.

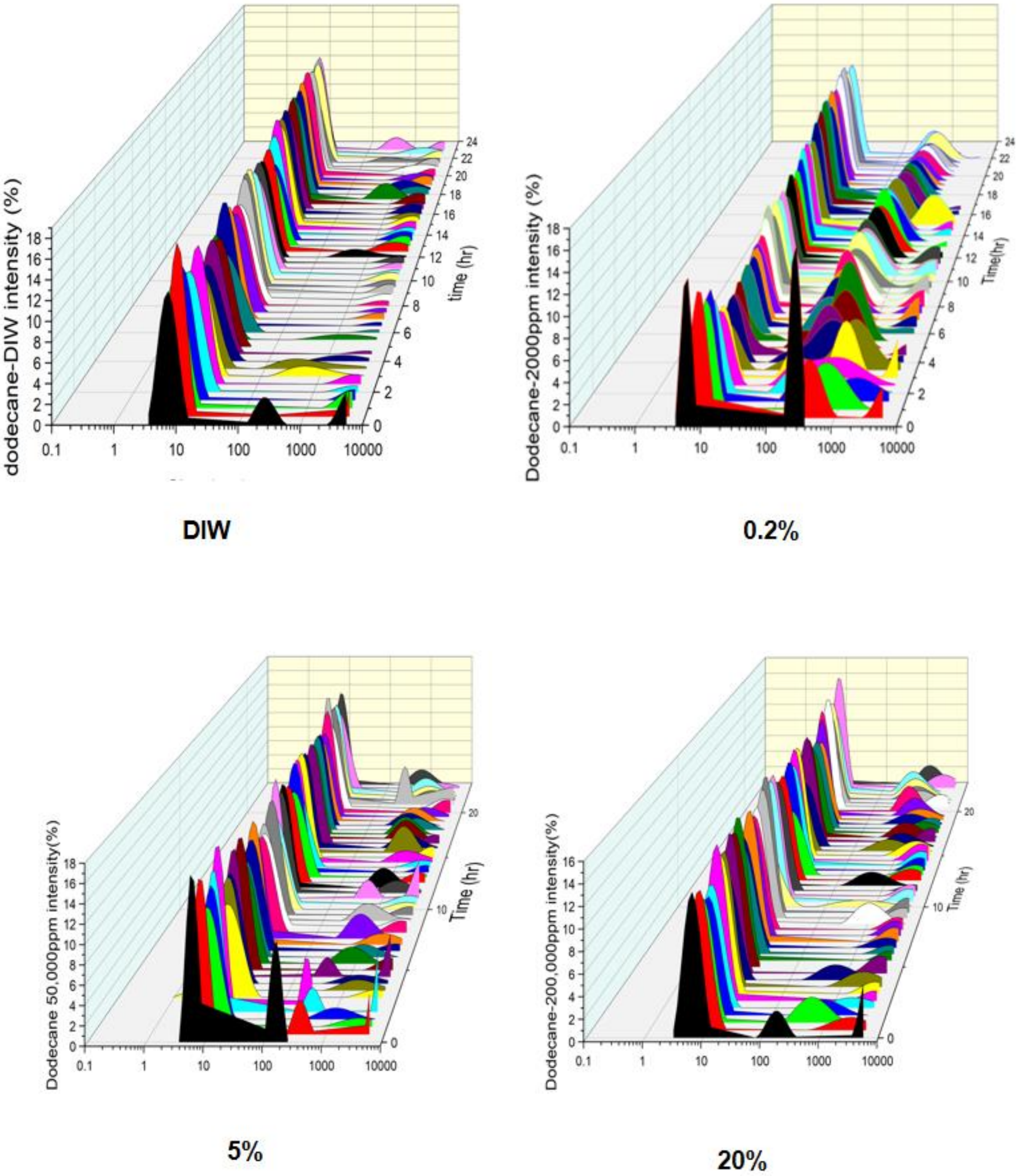

DIW

0.2%

5%

20%

Fig. 52: The emulsion size distribution graphs for 1% SPAN80 dodecane with various salinity brines (0%, 0.2%, 5% and 20%)

5.3. Pendant drop experiment results

An experimental investigation of spontaneous emulsification is proposed with a water drop pendant in a refined oil environment with surfactant. In this experiment, the purpose is to observe the spontaneous emulsion generation process. The droplets appear darker with time due to emulsion accumulation at the droplet surface. The interfacial tension for the water droplets with various salinity range from 3.47 mN/m to 4.71 mN/m. For all kinds of oil composition, the lower the salinity, the higher the IFT. The measurements of different salinity water interfacial tension in different oil are listed at Table 3.

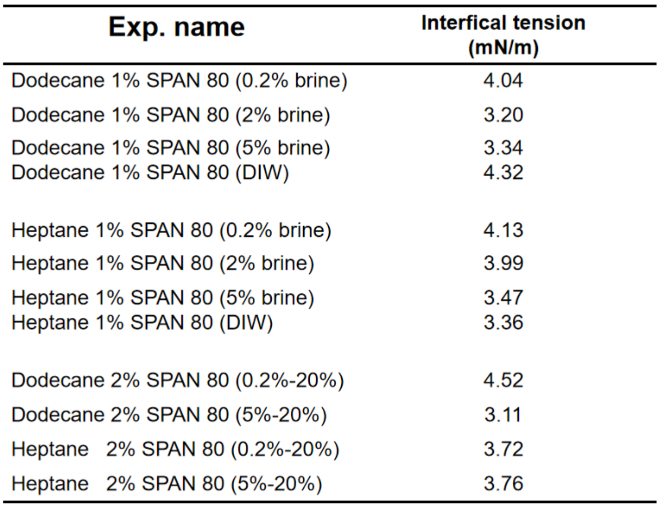

Exp. name	Interfical tension (mN/m)
Dodecane 1% SPAN 80 (0.2% brine)	4.04
Dodecane 1% SPAN 80 (2% brine)	3.20
Dodecane 1% SPAN 80 (5% brine)	3.34
Dodecane 1% SPAN 80 (DIW)	4.32
Heptane 1% SPAN 80 (0.2% brine)	4.13
Heptane 1% SPAN 80 (2% brine)	3.99
Heptane 1% SPAN 80 (5% brine)	3.47
Heptane 1% SPAN 80 (DIW)	3.36
Dodecane 2% SPAN 80 (0.2%-20%)	4.52
Dodecane 2% SPAN 80 (5%-20%)	3.11
Heptane 2% SPAN 80 (0.2%-20%)	3.72
Heptane 2% SPAN 80 (5%-20%)	3.76

Table 4: The interfacial tension for pendant water droplets in different oil

Fig. 51 illustrates stages of the spontaneous emulsification. The opacity of water drops increases as the time goes by, as micro-emulsion generates on the surface of the water droplets (Fig. 53a to Fig. 53b). the emulsion layer become thicker, and micelles accumulate with time. The micro-emulsion then accumulates and form protuberance on the surface. From Fig. 53 c we can observe that after 8.5 hours the opacity of the droplet is not uniform anymore, which is assumed to be caused by the protuberance. By gravity, the large protruding part will detach from the water droplet, leading to shrinkage of the droplet. Water will diffusing into the oil phase may also lead to the shrinkage [51].

The size of the micro-droplets in the pendant drop experiment (Fig. 53d) is around 1μm, which is very similar with the measurements of micro-droplets that we got from the microfluidic experiments (Fig. 47). Considering with the microfluidic condition where under the salinity gradient between the HSW and the LSW, the micelles can transport away from the LSW side so that there are always new micelles generates at the LSW side. The size of the droplets is similar with the early stage of the natural developing condition. If the amount of the transporting micelles lower than the amount of generating, the micelles will accumulate at the LSW/oil interface. So, these images give us another view of the emulsion generation process in the microfluidic throats and can help us better understanding the spontaneous emulsification on the pore scale.

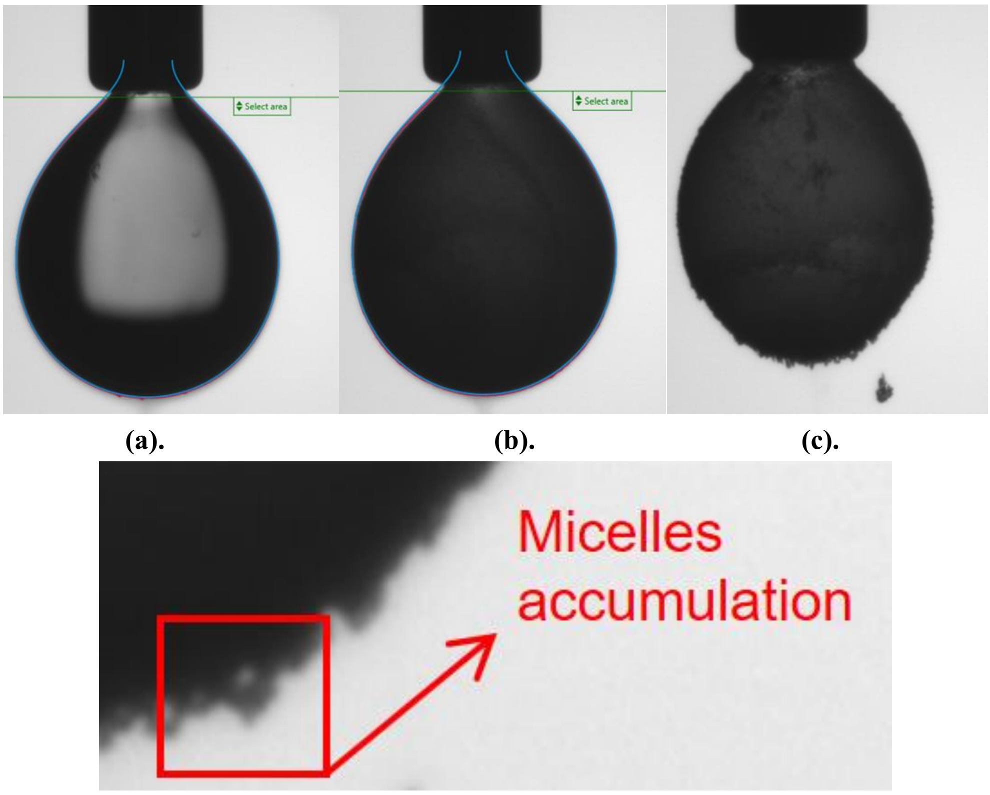
Select area
Select area
Micelles
accumulation

(a). (b). (c).

(d).

Fig. 53: Shape of the pendant drop for Dodecane 1% SPAN 80-1700 ppm at different time. (a).0.5 h (b). 1.5 h (c). 8.5 h. The diameter of the needle is 0.5 mm.

6. Discussion

In this section, we will first discuss how the salinity, oil properties and surfactants affect the water transportation performance in oil based on the results we got from the microfluidic experiments. Then, with the photos from the pendant drop experiments and the measurements offered with DLS, the water diffusion and transportation theory in the LSW/oil/HSW system will be investigated.

6.1. LSW Salinity

The effect of a salinity difference for water transport through a semi- membrane oil film is shown in Fig. 50 below. Both pure n-alkane and surfactants added n-alkane are shown to have the characteristics to be a semi-membrane film. To determine the performance of the water transport, 0.2% salt brine and 5% salt brine are selected for different oil composition. From Fig. 50, it is clear that more water pass through the oil film with a higher salinity gradient for all cases. It should be noted that we did not try all different salinities to find the optimum LSW but are mainly comparing two salinity gradients to see their effects. Larger salinity gradient indeed has a better performance for the water transportation.

For pure n-alkane, the final corrected relative area difference for dodecane between 0.2% brine and 5% brine is 0.6 and for heptane is 1.8. The heptane shows more sensitivity to the salinity gradient change. Depending on the specific situation, the growth of the HSW zone stopped diminished over time. We did not observe reduced growth with time for the 0.2% brine case, as most of the observed HSW zone ended up connected to the LSW. For surfactants added cases, the growth tendency is more similar between 0.2% and 5% salts content. Both heptane and dodecane with 1% SPAN80 reach a relative area difference of 0.4 at 40 hours. The relative area growth gradient is shown in Table 4, which indicates the water transportation rate. We can see that the pure heptane with 0.2% brine injection have the highest water transport rate, 14 times larger than the 5% brine case. The gradients for dodecane have less difference between these two salinities. This gives the same conclusion as Naeem and Aldousary, who stated that heptane has the best semi-permeable properties as a membrane under a salinity gradient situation [10, 35]. After adding surfactants, the methods for water transport are different from the pure n-alkane. It depends on the emulsion concentration and surfactants properties. In our experiments, both dodecane and heptane have similar performance with and without 1% SPAN 80 added to the oil.

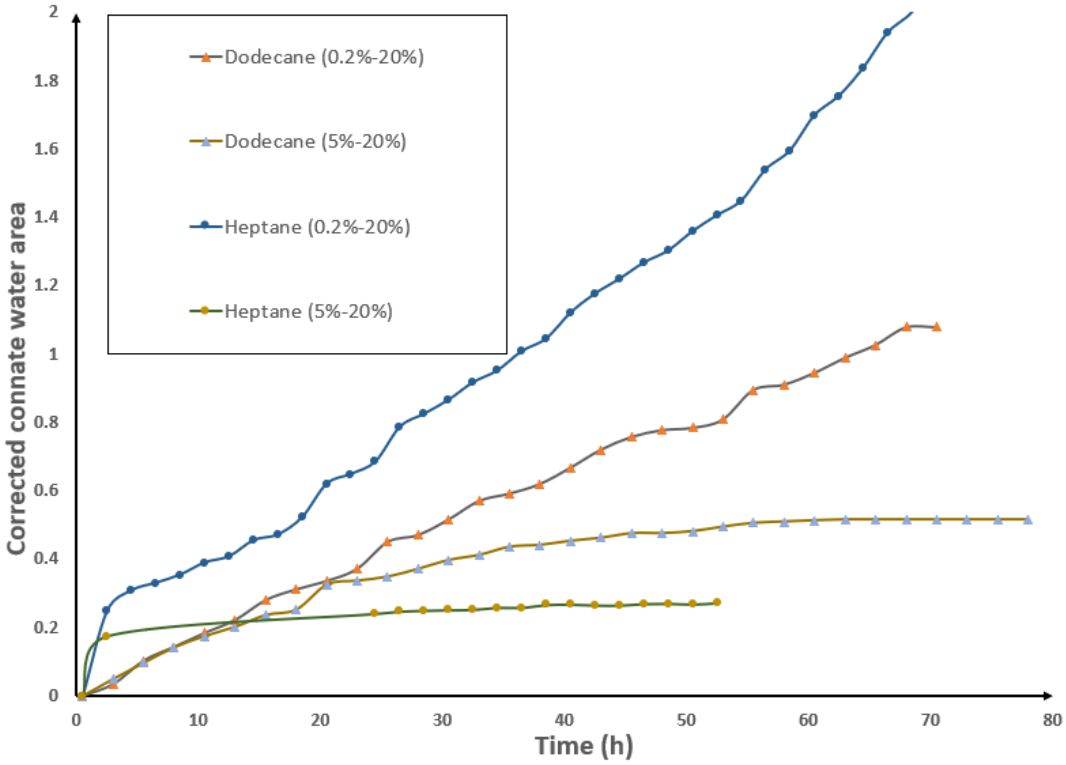

(a). Pure n-alkane

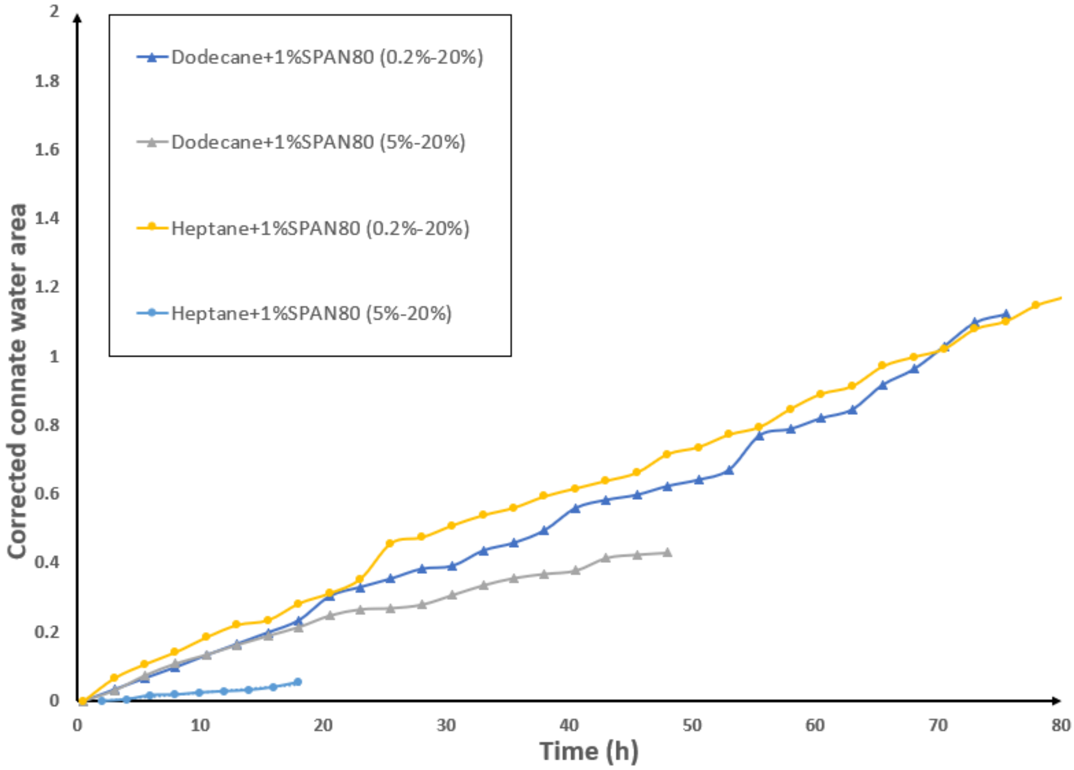

(b). 1% SPAN 80 n-alkane

Fig. 54: The curve of the HSW relative area growth in microfluidic experiments

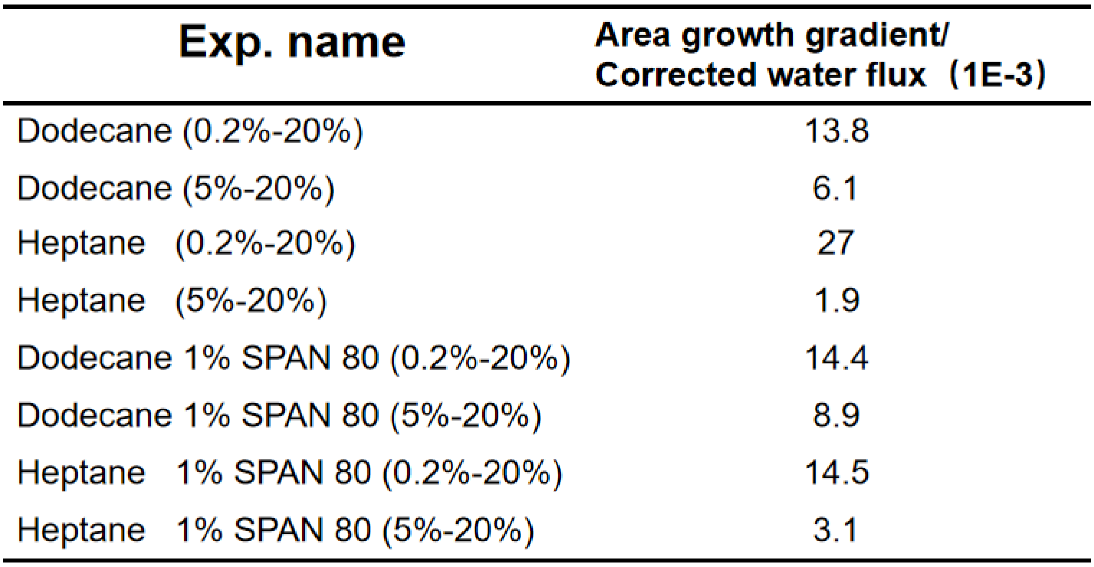

Exp. name	Area growth gradient/ Corrected water flux（1E-3)
Dodecane (0.2%-20%)	13.8
Dodecane (5%-20%)	6.1
Heptane (0.2%-20%)	27
Heptane (5%-20%)	1.9
Dodecane 1% SPAN 80 (0.2%-20%)	14.4
Dodecane 1% SPAN 80 (5%-20%)	8.9
Heptane 1% SPAN 80 (0.2%-20%)	14.5
Heptane 1% SPAN 80 (5%-20%)	3.1

Table 5: The relative area growth gradient for typical microfluidic experiments

6.2. Oil properties

From the microfluidic experiments, we can learn that the oil properties can highly affect the performance of oil as a semi-permeable membrane. In our experiments, the dodecane shows a weaker ability to let water transport comparing with the heptane, as Fig. 55 shown. The slope of the curves with heptane (dots) are higher than dodecane (triangle). The dodecane has 5 more alkyl groups than heptane, which make it has higher weight and lower solubility. Considering the work of Naeem and Fredrikson, who conducted capillary experiments with toluene, heptane and crude oil, the heptane showed the optimum ability on water transportation even through toluene has a much higher water solubility[13] [35]. Our work supports their conclusion. It is still unclear how the water solubility in oil affects water transportation through the oil.

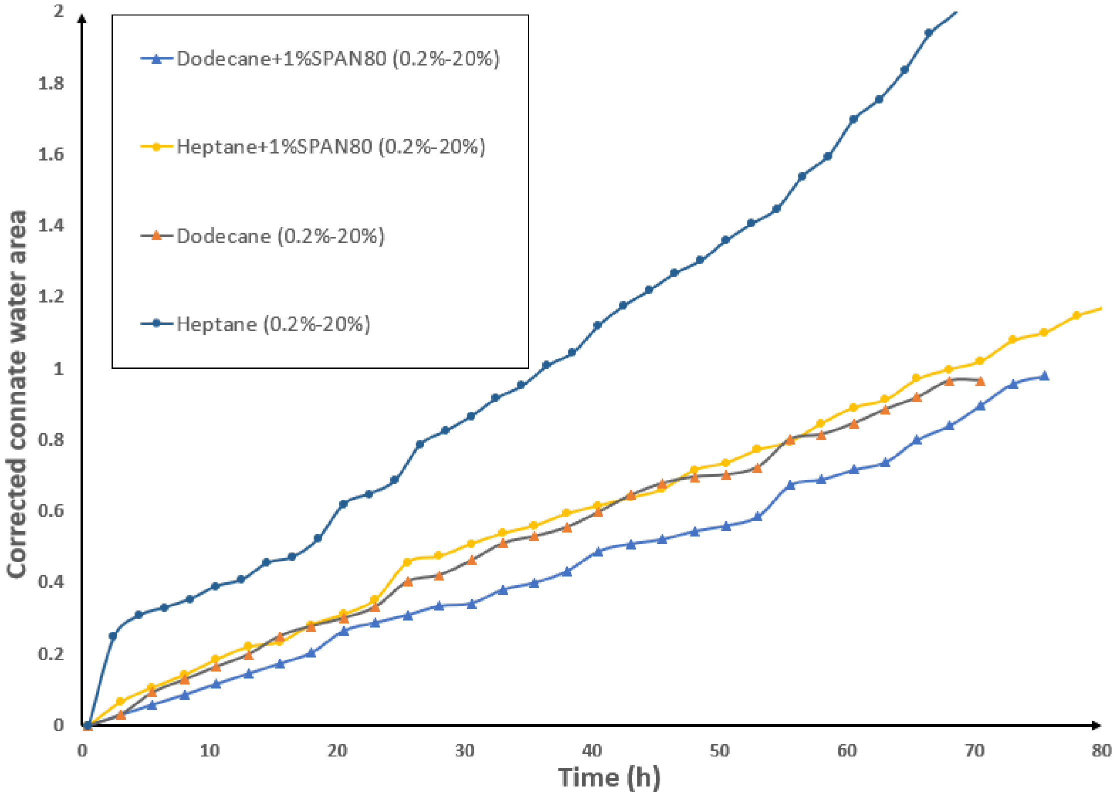

Fig. 55: Relative area curve for Dodecane and Heptane with and without surfactants

Before 24 hours, the surfactants added heptane shows a slightly higher water flux than 1% SPAN 80 added dodecane. After 24 hours, the slopes for them are similar. The difference in the oil properties that plays a role in emulsification water transfer is mainly due to micelles properties and the oil viscosity. For spherical particles like emulsion micelles, the Stokes-Einstein equation is usually used to calculate the diffusion coefficient. Three parameters domain the diffusion rate: temperature, fluid viscosity and particles diameter. As the temperature is constant for all our experiments, the micelles size and the viscosity of the fluid are main factors to be considered. The micelles size for the heptane and the dodecane changes with the time. By DLS experiments we can study how the emulsion size changes with time in a steady environment. It should be noted that the difference between the DLS chamber and the microfluidic is that the emulsions transport in the oil phase directionally in microfluidic experiments. In this circumstance, if there is enough surfactant supply for the emulsification, the emulsion size in the microfluidic can be assumed similar to the size at early times in DLS. As Fig. 56 shows, the small emulsion proportion for heptane in the early stage (at the first 2 hours) is far less than dodecane. By the Stokes-Einstein equation, the smaller the particles the higher transport rate they have. The emulsion generates in the dodecane thus have a better ability to transport water through the oil phase. It also explains why the heptane is less viscous but have the similar water transportation effects.

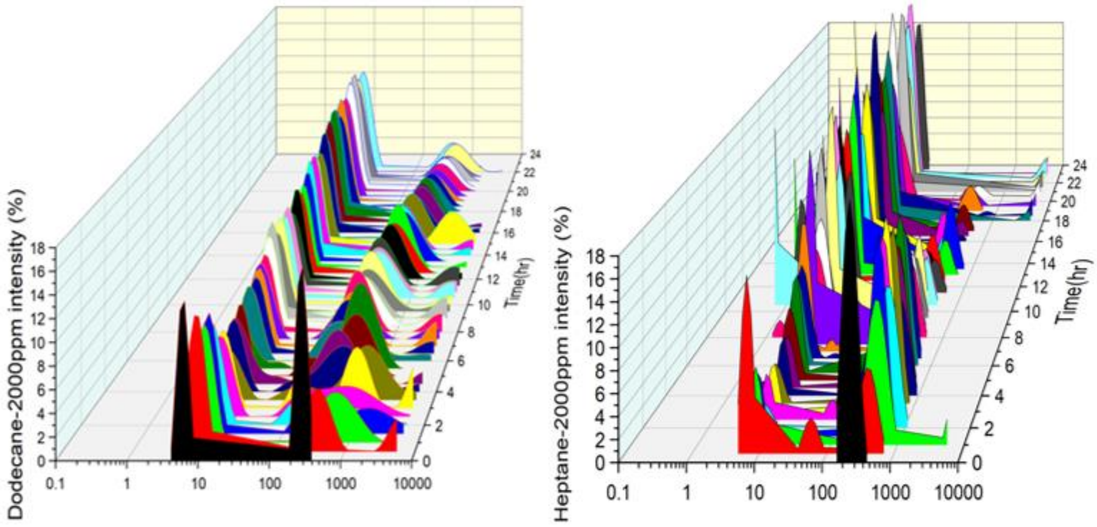

Fig. 56: The emulsion size distribution vis time for heptane and dodecane

6.3. Surfactant concentration

Different surfactant concentrations were used in our microfluidic experiments. Fig. 57 shows corrected relative area versus time for n-alkane with 0, 1% and 2% w/w SPAN 80. We can see that the slope of the curve for dodecane is 2%> 0%> 1%, while for heptane is 2% ≈0% >1%. The results do not fit with the assumption that more surfactants give higher diffusion rate. The water transportation rate in pure heptane is higher than the heptane with low concentration surfactants added. It can be concluded that the emulsification inhibits the molecular osmosis effect. The emulsification, which is the process of water packed as the micelles, captures large amount of the diffused water molecules, preventing them from transporting through the oil film. The micelles in heptane diffuse slower than the water molecules, which causes a lower water flux. This conclusion is not absolute, as dodecane with 2% SPAN 80 added shows a highest water flux. It is still hard to get the conclusion that the water directly diffusion and the emulsion transportation are coexistent under this situation.

The same is, for both heptane and dodecane, an appropriately higher surfactant concentration can indeed increase the water transportation rate in synthetic oil. Comparing with the heptane, the dodecane is less sensitive to the surfactant's concentration change. The surfactants concentration more domain the water flux as the increase of oil viscosity. It should be noted that the viscosity of heptane is 0.42 cp, toluene is 0.55 cp and dodecane is 1.98 cp. It is observed that the higher viscosity of the oil the lower of the water transportation rate due to the osmosis, and more influence by surfactants concentration. However, this conclusion still needs more experiments to support.

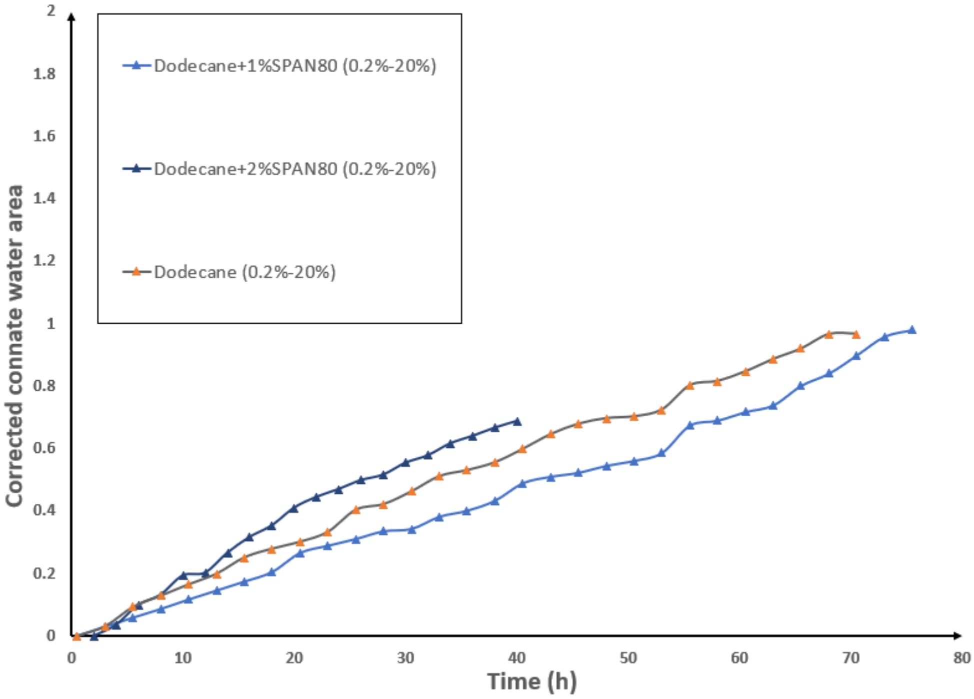

(a). Dodecane with 0%, 1% and 2% SPAN 80

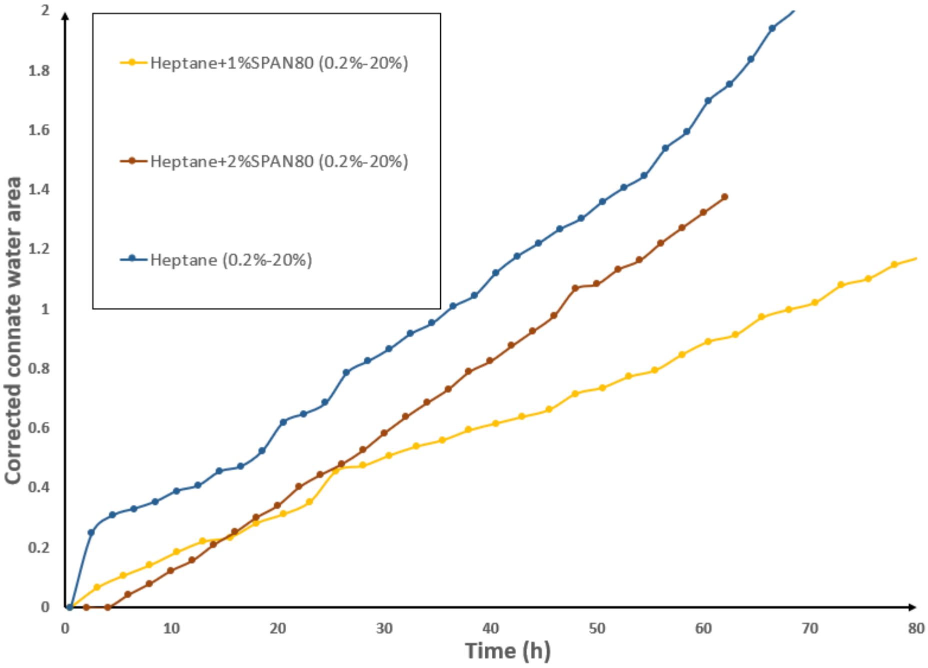

(b). Heptane with 0%, 1% and 2% SPAN 80

Fig. 57: HSW relative area curve for dodecane and heptane with 0, 1% and % w/w SPAN 80

7. Conclusions and future research advice

In this study, ideal 2-D microfluidic experiments were investigated to study osmosis and emulsification as underlying mechanisms to enhance oil recovery during low salinity water flooding. In our experiment, an oil wet system was used to observe connate water swelling. By setting different salinity of brines as injected LSW, the connate water expands of different roles. From our calculations, the diffusion theory cannot fully explain the osmosis effect. More studies need to focus on the mechanisms of water transportation methods in the osmosis. Microfluidic experiments were set to study the effect of spontaneous emulsification during LSW flooding. By adding oil soluble surfactants like SPAN 80, emulsions will generate around the interface between LSW and oil. However, it is difficult to quantify the emulsions effect and understand the inner mechanisms. The DLS and pendant drop observation experiments were conducted to help us better understand spontaneous emulsification. Through our studies, several inferences can be determined:

(1) Hydrocarbon can play the role as a semi-membrane so that water molecules can pass through the oil phase under a salinity gradient. The larger the water salinity gradient in two side, the higher the water diffusion rate. As a result, when the oil phase contacts LSW, enclosed high salinity connate water can expand, causing the oil mobilization.

(2) A supersaturation zone due to spontaneous emulsification was observed at the LSW/oil interface when the oil contains surfactants. The surfactants, generating reverse micelles by enveloping diffused water molecules, which should have higher transportation rate in oil film. Spontaneous emulsification inhibits water transportation due to the osmosis effect in synthetic oil, causing a slower water flux. It is still not clear that whether the coexistent of the water transportation caused by the osmosis and spontaneous emulsification in high viscous oil, crude oil for instance.

(3) The experiment with heptane shows a higher water transportation rate than the dodecane for both osmosis and spontaneous emulsification, which support the conclusion from previous studies. The connections between water transportation rate and oil properties such as viscosity and water solubility are need more studies.

The mechanisms of water transport in oil by osmosis are still unclear. More case study with different salinity brines and different types of oil are needed. We conducted the microfluidic experiments under a rock-pore structure to simulate a real LSW injection. This structure inhibits the quantification of the effects. A capillary microfluidic system is more suitable for quantification. Further, it would be beneficial to find a method to monitor the water transportation process in the oil phase at real time, which can quantify the individual effects of emulsion transport and molecular diffusion transport.

8.Bibliography

[1] G. G. Bernard, "Effect of Floodwater Salinity on Recovery Of Oil from Cores Containing Clays," presented at the SPE California Regional Meeting, Los Angeles, California, 1967/1/1/, 1967. [Online]. Available: https://doi.org/10.2118/1725-MS.

[2] P. P. Jadhunandan and N. R. Morrow, "Effect of Wettability on Waterflood Recovery for Crude-Oil/Brine/Rock Systems," *SPE-22597-PA,* vol. 10, no. 01, pp. 40-46, 1995/2/1/ 1995, doi: 10.2118/22597-PA.

[3] H. O. Yildiz and N. R. Morrow, "Effect of brine composition on recovery of Moutray crude oil by waterflooding," *Journal of Petroleum Science and Engineering,* vol. 14, no. 3, pp. 159-168, 1996/05/01/ 1996, doi: https://doi.org/10.1016/0920-4105(95)00041-0.

[4] G.-Q. Tang and N. R. Morrow, "Influence of brine composition and fines migration on crude oil/brine/rock interactions and oil recovery," *Journal of Petroleum Science and Engineering,* vol. 24, no. 2, pp. 99-111, 1999/12/01/ 1999, doi: https://doi.org/10.1016/S0920-4105(99)00034-0.

[5] J. M. Schembre and A. R. Kovscek, "Mechanism of Formation Damage at Elevated Temperature," *Journal of Energy Resources Technology,* vol. 127, no. 3, pp. 171-180, 2005, doi: 10.1115/1.1924398.

[6] A. Lager, K. J. Webb, C. J. J. Black, M. Singleton, and K. S. Sorbie, "Low Salinity Oil Recovery - An Experimental Investigation1," *SPWLA-2017-v58n1a3,* vol. 49, no. 01, p. 8, 2008/2/1/ 2008. [Online]. Available: https://doi.org/.

[7] T. Austad, A. Rezaeidoust, and T. Puntervold, "Chemical Mechanism of Low Salinity Water Flooding in Sandstone Reservoirs," presented at the SPE Improved Oil Recovery Symposium, Tulsa, Oklahoma, USA, 2010/1/1/, 2010. [Online]. Available: https://doi.org/10.2118/129767-MS.

[8] D. J. Ligthelm, J. Gronsveld, J. Hofman, N. Brussee, F. Marcelis, and H. van der Linde, "Novel Waterflooding Strategy By Manipulation Of Injection Brine Composition," presented at the EUROPEC/EAGE Conference and Exhibition, Amsterdam, The Netherlands, 2009/1/1/, 2009. [Online]. Available: https://doi.org/10.2118/119835-MS.

[9] M. Sohrabi, P. Mahzari, S. A. Farzaneh, J. R. Mills, P. Tsolis, and S. Ireland, "Novel Insights Into Mechanisms of Oil Recovery by Use of Low-Salinity-Water Injection," *SPE-179741-PA,* vol. 22, no. 02, pp. 407-416, 2017/4/1/ 2017, doi: 10.2118/172778-PA.

[10] S. Aldousary and A. R. Kovscek, "The diffusion of water through oil contributes to spontaneous emulsification during low salinity waterflooding," *Journal of Petroleum Science and Engineering,* vol. 179, pp. 606-614, 2019/08/01/ 2019, doi: https://doi.org/10.1016/j.petrol.2019.04.041.

[11] J. Liu, J. J. Sheng, and J. Tu, "Effect of spontaneous emulsification on oil recovery in tight oil-wet reservoirs," *Fuel,* vol. 279, p. 118456, 2020/11/01/ 2020, doi: https://doi.org/10.1016/j.fuel.2020.118456.

[12] K. Sandengen, A. Kristoffersen, K. Melhuus, and L. O. Jøsang, "Osmosis as Mechanism

for Low-Salinity Enhanced Oil Recovery," *SPE-179741-PA,* vol. 21, no. 04, pp. 1227-1235, 2016/8/1/ 2016, doi: 10.2118/179741-PA.

[13] S. B. Fredriksen, A. U. Rognmo, K. Sandengen, and M. A. Fernø, "Wettability Effects on Osmosis as an Oil-Mobilization Mechanism During Low-Salinity Waterflooding," *SPWLA-2017-v58n1a3,* vol. 58, no. 01, pp. 28-35, 2017/2/1/ 2017. [Online]. Available: https://doi.org/.

[14] P. Mahzari and M. Sohrabi, "Crude Oil/Brine Interactions and Spontaneous Formation of Micro-Dispersions in Low Salinity Water Injection," presented at the SPE Improved Oil Recovery Symposium, Tulsa, Oklahoma, USA, 2014/4/12/, 2014. [Online]. Available: https://doi.org/10.2118/169081-MS.

[15] M. Broens and E. Unsal, "Emulsification kinetics during quasi-miscible flow in dead-end pores," *Advances in Water Resources,* vol. 113, pp. 13-22, 2018/03/01/ 2018, doi: https://doi.org/10.1016/j.advwatres.2018.01.001.

[16] L. Yan, H. Aslannejad, S. M. Hassanizadeh, and A. Raoof, "Impact of water salinity differential on a crude oil droplet constrained in a capillary: Pore-scale mechanisms," *Fuel,* vol. 274, p. 117798, 2020/08/15/ 2020, doi: https://doi.org/10.1016/j.fuel.2020.117798.

[17] K. J. Webb, C. J. J. Black, and H. Al-Ajeel, "Low Salinity Oil Recovery - Log-Inject-Log," 2003. [Online]. Available: https://doi.org/10.2118/81460-MS.

[18] P. L. McGuire, J. R. Chatham, F. K. Paskvan, D. M. Sommer, and F. H. Carini, "Low Salinity Oil Recovery: An Exciting New EOR Opportunity for Alaska's North Slope," 2005. [Online]. Available: https://doi.org/10.2118/93903-MS.

[19] A. Katende and F. Sagala, "A critical review of low salinity water flooding: Mechanism, laboratory and field application," *Journal of Molecular Liquids,* vol. 278, pp. 627-649, 2019/03/15/ 2019, doi: https://doi.org/10.1016/j.molliq.2019.01.037.

[20] E. N. Pollen and C. F. Berg, "Experimental Investigation of Osmosis as a Mechanism for Low-Salinity EOR," presented at the Abu Dhabi International Petroleum Exhibition & Conference, Abu Dhabi, UAE, 2018/11/12/, 2018. [Online]. Available: https://doi.org/10.2118/192753-MS.

[21] J. Sheng, "Critical review of low-salinity waterflooding," *Journal of Petroleum Science and Engineering,* vol. 120, 08/01 2014, doi: 10.1016/j.petrol.2014.05.026.

[22] A. K. Alhuraishawy, B. Bai, M. Wei, J. Geng, and J. Pu, "Mineral dissolution and fine migration effect on oil recovery factor by low-salinity water flooding in low-permeability sandstone reservoir," *Fuel,* vol. 220, pp. 898-907, 2018/05/15/ 2018, doi: https://doi.org/10.1016/j.fuel.2018.02.016.

[23] M. Cissokho, H. Bertin, S. Boussour, P. Cordier, and G. Hamon, "Low Salinity Oil Recovery On Clayey Sandstone: Experimental Study," *SPWLA-2017-v58n1a3,* vol. 51, no. 05, p. 9, 2010/10/1/ 2010. [Online]. Available: https://doi.org/.

[24] E. Alagic and A. Skauge, "Combined Low Salinity Brine Injection and Surfactant Flooding in Mixed−Wet Sandstone Cores," *Energy & Fuels,* vol. 24, no. 6, pp. 3551-3559, 2010/06/17 2010, doi: 10.1021/ef1000908.

[25] W. Song and A. R. Kovscek, "Spontaneous clay Pickering emulsification," *Colloids and Surfaces A: Physicochemical and Engineering Aspects,* vol. 577, pp. 158-166,

2019/09/20/ 2019, doi: https://doi.org/10.1016/j.colsurfa.2019.05.030.

[26] C. T. Q. Dang, L. X. Nghiem, Z. J. Chen, and Q. P. Nguyen, "Modeling Low Salinity Waterflooding: Ion Exchange, Geochemistry and Wettability Alteration," presented at the SPE Annual Technical Conference and Exhibition, New Orleans, Louisiana, USA, 2013/9/30/, 2013. [Online]. Available: https://doi.org/10.2118/166447-MS.

[27] P. Vledder, J. C. Fonseca, T. Wells, I. Gonzalez, and D. Ligthelm, "Low Salinity Water Flooding: Proof Of Wettability Alteration On A Field Wide Scale," 2010. [Online]. Available: https://doi.org/10.2118/129564-MS.

[28] L. Mei, D. J. McClements, J. Wu, and E. A. Decker, "Iron-catalyzed lipid oxidation in emulsion as affected by surfactant, pH and NaCl," *Food Chemistry,* vol. 61, no. 3, pp. 307-312, 1998/03/31/ 1998, doi: https://doi.org/10.1016/S0308-8146(97)00058-7.

[29] W. O. Winsauer and W. M. McCardell, "Ionic Double-Layer Conductivity in Reservoir Rock," *SPE-953129-G,* vol. 5, no. 05, pp. 129-134, 1953/5/1/ 1953, doi: 10.2118/953129-G.

[30] S. Bhattacharjee, M. Elimelech, and M. Borkovec, "DLVO interaction between colloidal particles: Beyond Derjaguin's approximation," *Croatica Chemica Acta,* vol. 71, no. 4, pp. 883-903, 1998.

[31] R. A. Nasralla and H. A. Nasr-El-Din, "Double-Layer Expansion: Is It a Primary Mechanism of Improved Oil Recovery by Low-Salinity Waterflooding?," *SPE-154334-PA,* vol. 17, no. 01, pp. 49-59, 2014, doi: 10.2118/154334-PA.

[32] J. Yang *et al.*, "Wettability Alteration during Low-Salinity Waterflooding and the Relevance of Divalent Ions in This Process," *Energy & Fuels,* vol. 30, no. 1, pp. 72-79, 2016/01/21 2016, doi: 10.1021/acs.energyfuels.5b01847.

[33] K. Sandengen and O. J. Arntzen, "Osmosis During Low Salinity Water Flooding," 2013, doi: https://doi.org/10.3997/2214-4609.20142608.

[34] A. Emadi and M. Sohrabi, *Visual Investigation of Oil Recovery by LowSalinity Water Injection: Formation of Water Micro-Dispersions and WettabilityAlteration*. 2013.

[35] M. H. Towfighi Naeem and A. H. Saeedi Dehaghani, "Evaluation of the performance of oil as a membrane during low-salinity water injection; focusing on type and concentration of salts," *Journal of Petroleum Science and Engineering,* vol. 192, p. 107228, 2020/09/01/ 2020, doi: https://doi.org/10.1016/j.petrol.2020.107228.

[36] S. chemistry and Coatings, "Handbook of Applied Surface and Colloid Chemistry," *Pigment & resin technology,* vol. 35, no. 5, pp. 68-69, 2006, doi: 10.1108/prt.2006.12935eac.007.

[37] R. Martinez-Palou *et al.*, "Demulsification of heavy crude oil-in-water emulsions: A comparative study between microwave and thermal heating," (in English), *Fuel,* vol. 113, pp. 407-414, Nov 2013, doi: 10.1016/j.fuel.2013.05.094.

[38] A. A. Umar, I. B. M. Saaid, A. A. Sulaimon, and R. B. M. Pilus, "A review of petroleum emulsions and recent progress on water-in-crude oil emulsions stabilized by natural surfactants and solids," *Journal of Petroleum Science and Engineering,* vol. 165, pp. 673-690, 2018/06/01/ 2018, doi: https://doi.org/10.1016/j.petrol.2018.03.014.

[39] S. A. Berridge, R. A. Dean, R. G. Fallows, and A. Fish, "The properties of persistent oils at sea," *Journal of the Institute of Petroleum,* vol. 54, pp. 300-309, 1968.

[40] J. Sjöblom, L. Mingyuan, A. A. Christy, and T. Gu, "Water-in-crude-oil emulsions from the Norwegian continental shelf 7. Interfacial pressure and emulsion stability," *Colloids and Surfaces,* vol. 66, no. 1, pp. 55-62, 1992/09/21/ 1992, doi: https://doi.org/10.1016/0166-6622(92)80120-Q.

[41] M. Fingas, "Prediction of the Formation of Water-in-Oil Emulsions," ed. Cham: Cham: Springer International Publishing, 2015, pp. 57-83.

[42] M. Bergstrom, "Thermodynamics and Bending Energetics of Microemulsions," 2017.

[43] Y. Yamashita, R. Miyahara, and K. Sakamoto, "Chapter 28 - Emulsion and Emulsification Technology," in *Cosmetic Science and Technology*, K. Sakamoto, R. Y. Lochhead, H. I. Maibach, and Y. Yamashita Eds. Amsterdam: Elsevier, 2017, pp. 489-506.

[44] K. Holmberg, D. O. Shah, and M. J. Schwuger, *Handbook of applied surface and colloid chemistry : Vol. 1*. Chichester: Wiley, 2002.

[45] M. Mohammadi and H. Mahani, "Direct insights into the pore-scale mechanism of low-salinity waterflooding in carbonates using a novel calcite microfluidic chip," *Fuel,* vol. 260, p. 116374, 2020/01/15/ 2020, doi: https://doi.org/10.1016/j.fuel.2019.116374.

[46] C. Solans, D. Morales, and M. Homs, "Spontaneous emulsification," *Current Opinion in Colloid & Interface Science,* vol. 22, pp. 88-93, 2016/04/01/ 2016, doi: https://doi.org/10.1016/j.cocis.2016.03.002.

[47] J. C. López-Montilla, P. E. Herrera-Morales, S. Pandey, and D. O. Shah, "Spontaneous Emulsification: Mechanisms, Physicochemical Aspects, Modeling, and Applications," *Journal of Dispersion Science and Technology,* vol. 23, no. 1-3, pp. 219-268, 2002/01/01 2002, doi: 10.1080/01932690208984202.

[48] K. Chan and D. Shah, "The molecular mechanism for achieving ultra low interfacial tension minimum in a petroleum sulfonate/oil/brine system," *Journal of Dispersion Science and Technology - J DISPER SCI TECH,* vol. 1, pp. 55-95, 01/01 1980, doi: 10.1080/01932698008962161.

[49] M. Schmitt, R. Toor, R. Denoyel, and M. Antoni, "Spontaneous Microstructure Formation at Water/Paraffin Oil Interfaces," *Langmuir,* vol. 33, no. 49, pp. 14011-14019, 2017/12/12 2017, doi: 10.1021/acs.langmuir.7b02549.

[50] J. Bahtz, D. Z. Gunes, A. Syrbe, N. Mosca, P. Fischer, and E. J. Windhab, "Quantification of Spontaneous W/O Emulsification and its Impact on the Swelling Kinetics of Multiple W/O/W Emulsions," *Langmuir,* vol. 32, no. 23, pp. 5787-5795, 2016/06/14 2016, doi: 10.1021/acs.langmuir.6b00425.

[51] M. Schmitt, R. Toor, R. Denoyel, and M. l. Antoni, "Spontaneous Microstructure Formation at Water/Paraffin Oil Interfaces," *Langmuir,* vol. 33, no. 49, pp. 14011-14019, 2017, doi: 10.1021/acs.langmuir.7b02549.

[52] I. Fatt, "Influence of Dead-End Pores on Relative Permeability of Porous Media," *Science,* vol. 134, no. 3492, p. 1750, 1961, doi: 10.1126/science.134.3492.1750.

[53] S. Mohammadi, H. Mahani, S. Ayatollahi, and V. Niasar, "Impact of Oil Polarity on the Mixing Time at the Pore-Scale in Low Salinity Waterflooding," *Energy & Fuels,* 09/16 2020, doi: 10.1021/acs.energyfuels.0c01972.

[54] B. P. Binks and J. H. Clint, "Solid wettability from surface energy components: relevance to Pickering emulsions," *Langmuir,* vol. 18, no. 4, pp. 1270-1273, 2002.

[55] B. Wei *et al.*, "Influence of Individual Ions on Oil/Brine/Rock Interfacial Interactions and Oil–Water Flow Behaviors in Porous Media," *Energy Fuels,* vol. 31, no. 11, pp. 12035-12045, 2017, doi: 10.1021/acs.energyfuels.7b02458.

[56] M. J. Rosen and J. T. Kunjappu, *Surfactants and interfacial phenomena*. John Wiley & Sons, 2012.

[57] C. A. Miller, "Spontaneous Emulsification Produced by Diffusion — A Review," *Colloids and Surfaces,* vol. 29, no. 1, pp. 89-102, 1988/01/01/ 1988, doi: https://doi.org/10.1016/0166-6622(88)80173-2.

[58] C. E. Perles, P. L. O. Volpe, and A. J. F. Bombard, "Study of the Cation and Salinity Effect on Electrocoalescence of Water/Crude Oil Emulsions," *Energy & Fuels,* vol. 26, no. 11, pp. 6914-6924, 2012/11/15 2012, doi: 10.1021/ef301433m.

[59] P. Rostami, M. F. Mehraban, M. Sharifi, M. Dejam, and S. Ayatollahi, "Effect of water salinity on oil/brine interfacial behaviour during low salinity waterflooding: A mechanistic study," *Petroleum,* vol. 5, no. 4, pp. 367-374, 2019/12/01/ 2019, doi: https://doi.org/10.1016/j.petlm.2019.03.005.

[60] V. Kislik, *Liquid Membranes: Principles and Applications in Chemical Separations and Wastewater Treatment*. 2009.

[61] A. Einstein, "Über die von der molekularkinetischen Theorie der Wärme geforderte Bewegung von in ruhenden Flüssigkeiten suspendierten Teilchen," *Annalen der Physik,* https://doi.org/10.1002/andp.19053220806 vol. 322, no. 8, pp. 549-560, 1905/01/01 1905, doi: https://doi.org/10.1002/andp.19053220806.

[62] J. T. Edward, "Molecular volumes and the Stokes-Einstein equation," *Journal of Chemical Education,* vol. 47, no. 4, p. 261, 1970/04/01 1970, doi: 10.1021/ed047p261.

[63] P. Goyal and V. Aswal, "Micellar structure and inter-micelle interactions in micellar solutions: Results of small angle neutron scattering studies," *Current Science,* vol. 80, 04/25 2001.

[64] H. Mahani, A. L. Keya, S. Berg, W.-B. Bartels, R. Nasralla, and W. R. Rossen, "Insights into the Mechanism of Wettability Alteration by Low-Salinity Flooding (LSF) in Carbonates," *Energy & Fuels,* vol. 29, no. 3, pp. 1352-1367, 2015/03/19 2015, doi: 10.1021/ef5023847.

[65] S. Ahmadikhamsi, F. Golfier, C. Oltean, E. Lefèvre, and S. A. Bahrani, "Impact of surfactant addition on non-Newtonian fluid behavior during viscous fingering in Hele-Shaw cell," *Physics of Fluids,* vol. 32, no. 1, p. 012103, 2020/01/01 2020, doi: 10.1063/1.5128589.

[66] A. T. Hubbard, *Encyclopedia of surface and colloid science : Vol. 4 : Por-Z*. New York: Marcel Dekker, 2002.